Politecnico di Torino

Politecnico di Torino

Corso di Laurea

A.a. 2024/2025

Sessione di laurea Ottobre 2025

Modelling gas hydrates in a saline environment for water treatment and CO2 and N2 capture

Relatori:

Samir Bensaid

Baptiste Bouillot

Candidati:

Mirko Bove

Abstract

The study of clathrates as a solution for CO_2 capture and treatment has received significant scientific attention, as has their use in water desalination, a critical issue in many countries due to the scarcity of potable water. This work proposes a thermodynamic modeling approach compared with experimental data for the treatment of clathrate hydrates with N_2–CO_2 gas mixtures, using cyclopentane as an effective promoter. The binary equilibria among the considered substances were studied using the PPR78 model as an alternative to the simple Peng–Robinson (PR) and Soave–Redlich–Kwong (SRK) models. Thanks to the modifications introduced to the PR model, using PPR78 results in absolute standard deviations below 2%, making it an optimal model for the considered binary equilibria. For the modeling of hydrate formation, the van der Waals–Platteuw model was adopted, which, based on the Kihara parameters, allows the analysis of different chemical equilibria under varying pressure and temperature conditions. All binary mixtures of carbon dioxide, nitrogen, and cyclopentane during clathrate hydrate formation were examined, and results comparable with experimental data were obtained only for the binary equilibria containing the promoter; the lack of useful experimental data and computational difficulties prevented tracking the equilibrium behavior of nitrogen and carbon dioxide under varying pressure and temperature. A better estimation of the Kihara parameters and further experiments would allow an efficient analysis of the previously considered equilibrium; with parameter optimization, it would also be possible to consider the ternary complex of guest molecules during clathrate formation and the addition of salts typically present in water to improve the optimization process.

Summary

Formazione dei clatrati

L'acqua dolce è sempre stata una risorsa preziosa per la vita umana ed è stata storicamente facilmente disponibile, almeno fino a quando non è diventato evidente che a causa della crescita demografica, dell'industrializzazione e del riscaldamento globale è diventata una risorsa necessaria ma insufficiente. Per cercare di superare questo problema, si sono studiate e create differenti tecniche per provare a rendere l'acqua salata o dolce in potabile, o per lo meno con una purezza elevata, grazie a processi di desalinizzazione dell'acqua, ma che non sono ancora sufficienti a soddisfare le esigenze quotidiane dell'essere umano. Alcuni dei metodi comunemente studiati dalla comunità scientifica includono la distillazione termica, la distillazione inversa, l'osmosi, il congelamento ed elettrodialisi. Un'ulteriore ricerca, oggetto di questo lavoro, si concentra anche sulla desalinizzazione basata sugli idrati, che prova ad affronta il problema delle emissioni di CO_2, la cui eccessiva quantità oggi giorno richiede notevole attenzione. Pertanto, per le emissioni di CO_2, è stato studiato l'assorbimento attraverso idrati di clatrato. Gli idrati di clatrato, noti anche come idrati di gas, sono composti solidi cristallini e vengono creati ad alta pressione e basse temperature. Questi composti possono formare gabbie di diverse dimensioni, dentro le quali è possibile ospitare differenti molecole con caratteristiche differenti attraverso legami a idrogeno. A pressione atmosferica, anche molecole ospiti più pesanti possono produrre idrati di clatrato. Le molecole d'acqua e le molecole ospiti vengono combinate per generare una nuova fase solida durante la produzione di idrati per poi essere recuperati una volta divisi. I sali che entreranno all'interno delle gabbie che si creano durante il processo non andranno a formare una fase cristallina; quindi successivamente la dissociazione, l'acqua e le molecole ospiti potranno essere recuperate in forma pura. Il risultato principale atteso è acqua pura desalinizzata. Le molecole ospiti studiate in questo articolo per applicazioni di desalinizzazione sono il ciclopentano (Cp), anidride carbonica (CO_2) e azoto (N_2). Per completare il processo di desalinizzazione dell'acqua è necessario considerare sia sperimentalmente che teoricamente tutti i sali contenuti, ad esempio, nell'acqua di mare; dunque, data la complessità l'uso di questa tecnologia non è stato ancora

ottimizzato a causa di problemi di consumo e di immaturità tecnologica.

Ciclopentano

L'introduzione del ciclopentano all'interno del sistema per la formazione dei clatrati idrati è dovuta al fatto che presenta le caratteristiche per essere un promotore attendibile, soprattutto in condizioni di pressione atmosferica e basse temperature. Essendo un composto organico, il ciclopentano è immiscibile in acqua e quindi è facilmente recuperabile e riciclabile dopo la dissociazione per successivi riutilizzi. Dunque, il compito del ciclopentano è quello di fornire condizioni più favorevoli per la formazione di idrati.

Modelli termodinamici

Uno tra i più popolari metodi utilizzati per i calcoli (sia correlazioni che previsioni) dell'equilibrio di fase nelle miscele è l'utilizzo di equazioni di stato (EoS), poiché modelli di questo tipo descrivono al meglio le condizioni operative delle miscele in differenti intervalli di pressioni e determinate temperature, potendo considerare innumerevoli molecole differenti. Tra le tante equazioni di stato cubiche derivate dall'equazione di stato di van der Waals, i modelli presentati in questo lavoro sono quelli approfonditi da:

- Soave–Redlich–Kwong (SRK)
- Peng–Robinson (PR)

La differenza tra i due risulta notevole per la descrizione della fase d'equilibrio liquida e le rispettive densità, presentando per il modello PR un notevole adattamento per i composti idrocarburici e gassosi.

Ulteriori ricerche e confronti con vari modelli analizzati per i sistemi da approfondire hanno portato all'utilizzo di un modello aggiuntivo, il PR78, che corrisponde all'equazione predittiva di Peng–Robinson con le stesse regole di miscelazione ma presenta un'equazione diversa per il calcolo delle interazioni binarie (k_{ij}).

Ecco il calcolo delle interazioni binarie per il seguente modello:

$$k_{ij} = -\frac{1}{2}\sum_{k=1}^{N_g}\sum_{l=1}^{N_g}(\alpha_{ik}-\alpha_{jk})(\alpha_{il}-\alpha_{jl}) \cdot \frac{-A_{12}\left(\frac{298.15}{T}\right)^{\frac{A_{12}}{B_{1K}}} - 1 - \left(\frac{\sqrt{a_i}}{b_i} - \frac{\sqrt{a_j}}{b_j}\right)^2}{\frac{2\sqrt{a_i a_j}}{b_i b_j}} \tag{1}$$

con $k_{ii} = 0$

Nell'equazione precedente, T è la temperatura del sistema e a_i e b_i vengono calcolati semplicemente utilizzando le equazioni del modello PR78, utilizzate anche nelle equazioni per le regole di miscelazione. N_g è il numero di gruppi diversi definiti dal metodo (in questo lavoro risulterà essere uguale a due nel caso di equilibri binari). α_{ik} è la frazione della molecola i occupata dal gruppo k, dove si è imposto che $A_{kl} = A_{lk}$ e $B_{kl} = B_{lk}$ (dove k e l sono due gruppi diversi) e sono parametri costanti e inoltre l'occupazione dello stesso gruppo risulta essere uguale a zero, $A_{kk} = B_{kk} = 0$. Il parametro k_{ij} tra due molecole i e j ad una temperatura scelta, risulta inoltre dipendere da: la temperatura critica di entrambi i componenti (T_c), la pressione critica di entrambi i componenti (P_c) e il fattore acentrico di ciascun componente (ω).

Table 1: Dati critici e fattore acentrico per anidride carbonica, azoto e ciclopentano

Componenti	T_c **(K)**	P_c **(bar)**	ω
Anidride carbonica	304,21	73,83	0,224
Azoto	126,2	34,0	0,0377
Ciclopentano	511,7	45,1	0,195

Equilibri chimici bianri

Lo scopo della modellizzazione degli equilibri chimici tra i vari componenti considerati è quello di ottenere risultati ottimali per i coefficienti di fugacità, in differenti condizioni operative di pressione e temperatura sia per la fase liquida che vapore, utilizzati successivamente per la modellizzazione dei clatrati idrati.

Per ogni coppia di componenti si sono confrontati tutti e tre i modelli presentati laddove si sono raggiunti dei risultati congrui con gli esperimenti, condotti in differenti misure da diversi autori; i seguenti equilibri sono:

1. CO_2 e Ciclopentano
2. N_2 e Ciclopentano
3. CO_2 e N_2

Equilibrio binario tra CO_2 e Ciclopentano

Per l'equilibrio chimico tra anidride carbonica e ciclopentano si sono analizzate tre diverse condizioni operative, rispettivamente alla temperatura di 344.7 , 310.86 e 276.64 K con differenti range di pressione. Si riassumono i risultati delle analisi nella tabella 2 :

Modello	T (K)	P (bar)	K_{ij}	I_{ij}	ADD_x	ADD_y
SKR	344.7	9–101	0.129	0.03	\	\
	310.86	0–35	0.129	0.03	\	\
	276.64	1–65	0.129	0.03	-0.153	0.063
PR	344.7	9–101	0.119	-0.038	0.0277	0.0428571
	310.86	0–35	0.119	-0.038	0.1020857	0.036
	276.64	1–65	0.119	-0.038	0.522	0.025
PR78	344.7	9–101	-0.032	\	0.019	-0.007
	310.86	0–35	-0.002	\	0.031	-0.038
	276.64	1–65	-0.006	\	-0.045	-0.045

Table 2: Dati per la modellizzazione dell'equilibrio binario CO_2+CP.

Analizzando i risultati in tabella si nota come il modello SKR non riesce a risolvere in modo efficiente l'equilibrio dei componenti, mentre nel caso delle basse temperature invece si ottengono dei risultati per l'equilibrio ma presenta una deviazione standard elevata rispetto ai modelli successivi. Infatti, i modelli PR e PR78 riescono in tutti i casi a simulare il comportamento all'equilibrio avendo anche in alcuni casi un ADD inferiore al 2% sia per la fase liquida che gassosa. Si sottolinea anche come il coefficiente di interazione binaria, grazie alle modifiche introdotte con il modello PR78 variano in funzione della temperatura e presentano dei valori che si distaccano da quelli teorici avuti per il modello non modificato.

Equilibrio binario tra N_2 e Ciclopentano

Il secondo equilibrio chimico approfondito è tra azoto e ciclopentano dove si sono tenute in considerazione due diverse condizioni operative, rispettivamente alla temperatura di 410.2 e 366.4 K a differenti intervalli di pressione. Si riassumono i risultati delle simulazioni nella tabella 3:

Per il seguente equilibrio, i dati sperimentali sono presentati solo con temperature elevate data la complessità dell'equilibrio e di fatto anche l'intervallo di pressione

Model	T (K)	P (bar)	k_{ij}	ADD_x	ADD_y
SKR	410.2	9.21–180.45	\	0.047	0.00395
	366.4	13.2–178.17	\	0.137	0.007
PR	410.2	9.21–180.45	0.047	-0.015	0.004
	366.4	13.2–178.17	0.01	-0.003	-0.028
PR78	410.2	9.21–180.45	0.1048	0.006	0.009
	366.4	13.2–178.17	0.093	-0.0001	0.023

Table 3: Dati per la modellizzazione dell'equilibrio binario N_2+CP.

risulta variare tra i 10 e 180 bar. Tutti i modelli hanno riportato risultati utili per la simulazione dell'equilibrio tra azoto e ciclopentano, dove il modello che tende ad eguagliare maggiormente i dati sperimentali risulta essere il PR78 presentando una deviazione standard lato liquido inferiore dell'un percento mentre per la temperatura di 366.4 K tende leggermente ad essere superiore per il lato vapore. Anche in questo caso i coefficienti binari del modello PR78 si differenziano notevolmente dai valori teorici per il PR, dipendendo quindi l'equilibrio maggiormente dalle condizioni operative. Il modello SKR rimane un modello valido ma con deviazione standard lato liquido poco accettabile rispetto alle altre possibili varianti.

Equilibrio binario tra N_2 e CO_2

Infine, l'ultima miscela considerata è tra ciclopentano e azoto dove sono prese in oggetto tre diverse condizioni operative, rispettivamente alla temperatura di 288.3, 273.3 e 218.15 K con differenti intervalli di pressione. Si riassumono i risultati delle analisi nella tabella 4:

Dai risultati ottenuti in tabella, si notano come a differenti temperature l'intervallo di pressione sia differente soprattutto nel caso della temperatura maggiore a 288.3 K dove risulta molto piu restrittivo. Dalle analisi dei modelli si nota che per questo equilibrio, il modello PR non è in grado di risolvere l'equazioni per descrivere il comportamento all'equilibrio, ma grazie all'introduzione dei coefficienti binari del PR78, il modello risulta valido con simulazioni per ogni temperatura e intervallo di pressione considerato. Per comparare i modelli anche in questo caso si è confrontata la deviazione standard sia per il lato liquido che vapore, dove per la temperatura maggiore si presenta la deviazione standard minore registrata per entrambi i modelli che risultano pressoché comparabili. Al diminuire della temperatura si nota un aumento della deviazione standard per entrambe le fasi; quindi, il comportamento all'equilibrio tra azoto e anidride carbonica può essere descritto sia dal modello

Model	T (K)	P (bar)	K_{ij}	ADD_x	ADD_y
SKR	288.3	51.1–97	\	-0.0225	-0.009
	273.3	38.8–117	\	-0.0179	-0.0374
	218.15	7.71–132	\	-0.0142	-0.0404
PR	288.3	51.1–97	\	\	\
	273.3	38.8–117	\	\	\
	218.15	7.71–132	\	\	\
PR78	288.3	51.1–97	0.1101	0.0192	-0.0073444
	273.3	38.8–117	0.1104	0.0310	-0.0380
	218.15	7.71–132	0.1048	-0.045	-0.0458

Table 4: Dati per la modellizzazione dell'equilibrio binario CO_2+N_2.

SKR che PR78, dove uno risulta più adatto per temperature minore mentre l'altro per temperatura maggiori.

Equilibri chimici con formazione di clatrati

I dati sperimentali e la modellazione termodinamica svolgono un ruolo cruciale nello studio della formazione di idrati contenenti molecole ospiti; infatti, risultano esserci in letteratura differenti modelli ma si è scelto di approfondire la teoria di van der Waals e Platteuw per rappresentare la formazione di equilibrio di idrati contenenti le molecole ospiti considerate. Il modello di Van der Waals e Platteuw si basa sull'uguaglianza dei potenziali chimici dell'acqua nella fase idrato e nella fase liquida, solitamente rappresentati a partire da uno stato di riferimento che nella fase idrato corrisponde ad avere le cavità vuote :

$$\Delta\mu_w^{\beta-H} = \Delta\mu_w^{\beta-L} \tag{2}$$

Dove il potenziale chimico in fase liquida è calcolato con l'equazione di Gibbs-Duhem e il potenziale fase idrato è calcolato utilizzando la teoria di Van der Waals e Platteuw. Nella descrizione del metodo di Van der Waals e Platteuw si introdurrà un fattore, definito fattore di occupazione con formula :

$$\theta_j^i = \frac{C_j^i f_j(T,P)}{1+\sum_j C_j^i f_j(T,P)} \tag{3}$$

Il fattore di occupazione dipenderà dalla fugacità dei componenti, valori calcolati e analizzati precedentemente grazie all'uso dei modelli per interazione binaria dei componenti presi in analisi. L'applicazione di questa teoria richiede generalmente anche l'uso di parametri, denominati parametri di Kihara, che sono influenzati dalle proprietà molecolari e dall'affidabilità dei dati sperimentali. I valori utilizzati sono presi dalla letteraura e risultano essere :

Table 5: Parametri del potenziale di Kihara per le molecole guest considerate

Molecola	σ [Å]	ϵ/k_B [K]	a [Å]
CO_2	2.968	169.09	0.680
N_2	3.022	127.40	0.3526
Ciclopentano	2.72	265.5	0.8968

Dopo aver presentato il modello, si approfondiscono i risultati ottenuti dalle simulazioni del modello per gli equilibri chimici durante la formazione dei clatrati per le varie combinazioni di molecole considerate, le quali come precedentemente fatto sono:

1. CO_2 e Ciclopentano
2. N_2 e Ciclopentano
3. CO_2 e N_2

Equilibrio tra CO_2 e Cp con formazione di clatrati

Approfondendo lo studio dell'equilibrio chimico durate la formazione di idrato tra ciclopentano, promotore scelto per migliorare le condizioni di formazione e anidride carbonica, esso risulta essere quello maggiormente sperimentato. Infatti, in letteratura sono disponibili maggiori informazioni riguardante le composizioni di idrato per il sistema preso in considerazione al variare della temperatura e della pressione. La figura 1 mostra la comparazione tra dati i sperimentali e i dati della simulazione del modello per la formazione dei clatrati al variare di pressione e temperatura:

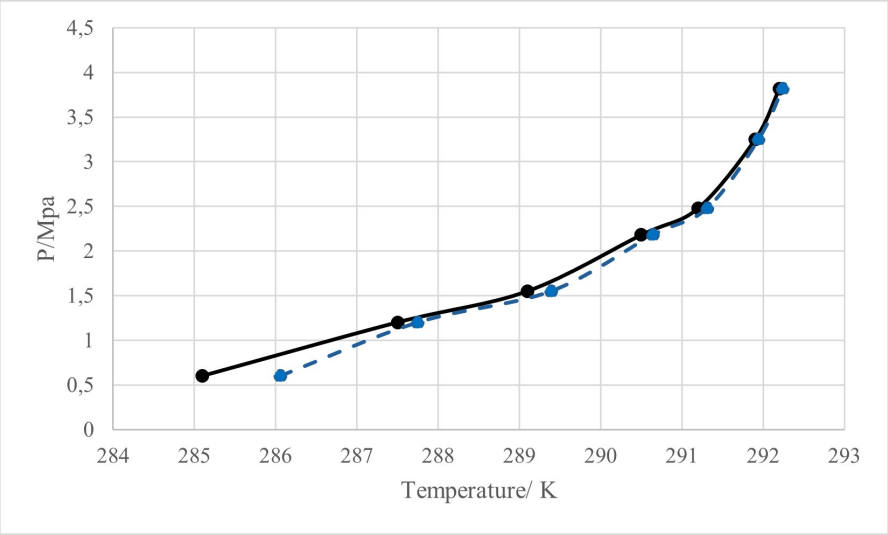

Figure 1: CO_2 + Cp curva di formazione clatrati; curva nera dati sperimentali, curva blu dati modello Van der Waals e Platteuw

Dalla figura, la curva nera rappresenta i dati sperimentali trovati in letteratura, invece la curva blu tratteggiata rappresenta i dati derivanti dalla simulazione. Al crescere di pressione e temperatura le curve hanno pressoché lo stesso andamento. Sottolineando anche la variazione di composizione tra le due sostanze, la quantità in frazione molare di anidride carbonica risulta essere maggiore di 0.96, aumentando con il crescere delle condizioni operative; quindi una piccola quantità di ciclopentano permette che il sistema abbia risultati validi dallo svolgimento delle equazioni del modello e che anche variando le condizioni operative possa permettere la formazione dei clatrati idrati adeguati.

Equilibrio tra N_2 e Cp con formazione di clatrati

L'equilibrio in fase idrato analizzato tra ciclopentano e azoto è il sistema più complesso, che grazie all'utilizzo dei coefficienti binari utilizzati, il modello idrato di Van der Waals e Platteuw e con i paramatri di Kihara adatti si è riuscito a rappresentare in Figura 2 la differenza tra i dati sperimentali e teorici dell'equilibrio considerato al variare delle condizioni del sistema:

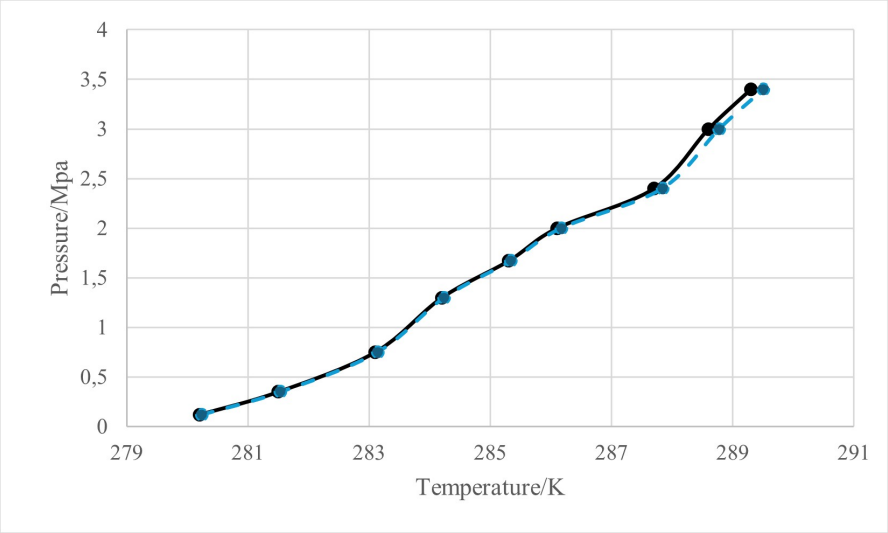

Figure 2: N_2 + Cp curva di formazione clatrati; curva nera dati sperimentali, curva blu dati modello Van der Waals e Platteuw

In figura 2 sono rappresentati con una curva nera continua i dati sperimentali ottenuti dalla letteratura, mentre la curva blu tratteggiata rappresenta la simulazione teorica del modello idrato che risulta essere comparabile. Di fatto, per questo equilibrio si ha una deviazione standard percentuale pari a 0.14%. Inoltre, si può affermare che il ciclopentano con ottime prestazioni da promotore, stabilizza l'equilibrio presentandosi con valori di frazioni molari basse che decrescono all'aumentare della temperatura e pressione.

Equilibrio tra CO_2 e N_2 con formazione di clatrati

Per l'ultimo equilibrio chimico in fase idrato tra anidride carbonica e azoto si sono analizzate ad una determinata temperatura le variazioni di composizione in fase idrato all'aumentare della pressione di azoto, comparate con i dati derivati dagli esperimenti ad temperatura fissa. Le fasi all'equilibrio risultano essere state approfondite alla temperatura di 274,277 e 280 K, risulta mostrato in figura 3 l'analisi a 274 K :

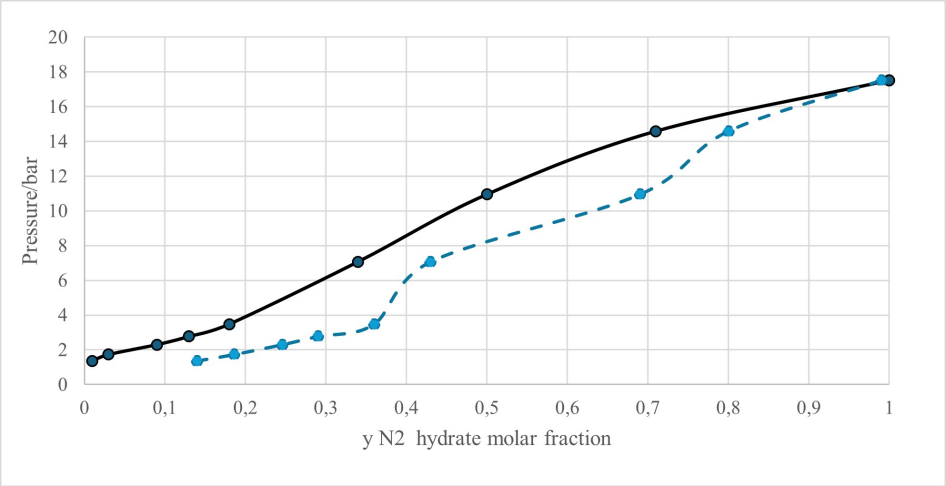

Figure 3: Confronto tra i risultati sperimentali e simulati per la frazione molare di idrato di N_2 nel sistema CO_2–N_2 in fase idrato a 274 K.

La rappresentazione seguente mostra con la linea nera, i dati sperimentali presi dalla letteratura della formazione di idrati contenenti azoto all'aumentare della pressione, considerando la composizione di anidride carbonica il complementare; la linea blu mostra i dati relativi alla simulazione teorica avente nel migliore dei casi una deviazione standard assoluta della fase gassosa pari a 0.12, ma l'andamento risulta confrontabile con i dati sperimentali. I risultati ottenuti sono dipendenti dai valori di Kihara scelti dalla letteratura che con le dovute accortezze potrebbero essere modificati e cercare di dimunire queste incongruenze.

Conclusione

Queste simulazioni teoriche, condotte con l'utilizzo di modelli alternativi e innovativi, hanno dimostrato che gli equilibri analizzati tra ciclopentano, anidride carbonica e azoto,inizialmente in condizioni di semplici equilibri binari in fase liquida e gassosa come componenti puri e successivamente in condizioni di formazione di clatrato idrato,risultano efficienti e comparabili con i dati sperimentali. I risultati ottenuti con il modello PR78, grazie al calcolo differente dei coefficienti binari che diventano dipendenti dalle condizioni operative, risultano i più efficienti, garantendo l'equilibrio anche con molecole aventi caratteristiche molto differenti. Infatti, il modello utilizzato principalmente per il calcolo dei coefficienti di fugacità, consente di ottenere ottimi risultati anche nel calcolo degli equilibri durante la formazione degli idrati; l'unico sistema che, per mancanza di dati sperimentali effettivi e per la sua complessità, non ha permesso di tracciare una curva al variare delle condizioni

operative è stato quello tra anidride carbonica e azoto. Inoltre, per tentare di creare un sistema ternario tra le tre molecole, sarebbe necessario approfondire l'equilibrio del sistema considerato e, successivamente, durante il calcolo della formazione degli idrati, introdurre differenti quantità di sali e confrontarle con i dati sperimentali.

Table of Contents

List of Tables

List of Figures

Chapter 1

Introduction

Clean water has always been a precious resource for human life and has historically been readily available, at least until it became apparent over a decade ago that it had become a critical resource due to population growth, industrialization, global warming, and for different countries, it has become a necessary but insufficient commodity [1]. There are already various techniques available for the water desalination process, but they are still not sufficient to meet the daily needs of a human being. Desalination, owing to the presence of seawater covering approximately 70% of the planet, has become an alternative and innovative method for producing fresh water [2]. Some of the commonly studied methods by the scientific community include thermal distillation, reverse osmosis, freezing, and electrodialysis [3, 4, 5]. For over a decade, research has also focused on hydrate-based desalination, which addresses the CO_2 emission problem. The emission of carbon dioxide (CO_2) from the combustion of fossil fuels has been identified as a substantial cause of global warming and ongoing climate change [6]. Valid technologies considered include carbon capture and storage (CCS), membrane separation, adsorption, and absorption [7, 8, 9], which have been identified as effective in selectively removing CO_2 from multicomponent gas streams, but still have some serious drawbacks. Thus, for cutting-edge CO_2 emissions for about a decade now, absorption through clathrate hydrates has been studied. Clathrate hydrates, also known as gas hydrates, are crystalline solid compounds that resemble ice and are created at high pressure and low temperatures. These compounds form cages around guest molecules through hydrogen bonding. There are different structures that can form during the formation of clathrate hydrates; the most common are Structure I, Structure II, and Structure H, each containing different numbers of cavities, which have been studied in detail by E. Sloan et al., 1998 [10]. Under atmospheric pressure, heavier guest molecules (such as tetrahydrofuran and cyclopentane (CP)) can produce clathrate hydrates. Water molecules and guest molecules are combined to generate a new solid phase during hydrate production.

They are recoverable once they are divided. Salts are also kept out of the crystalline phase. As a result, following dissociation, water and guest molecules can be retrieved. The main result expected is pure "desalinated" water. Clean water is obtained if the guest molecule can be isolated after dissociation. The guest molecules studied in this project for desalination applications are Cyclopentane (CP), Carbon dioxide (CO_2), nitrogen (N_2). To complete the process of desalinating water, it is necessary to consider both experimentally and theoretically all the salts contained, for example in seawater. There are several existing references that also deal with various systems containing different salts and promoters with different concentrations, but in this work the focus was on finding useful and coherent data with the introduction of the nitrogen molecule in each considered system, which presents challenging characteristics and has significant influence. Experimental data and thermodynamic modeling play a crucial role in investigating the formation of hydrates containing guest molecules. Over the years, various models have been presented like described from S. HoVan et al. [11], but in this article, it was chosen to focus on the classical theory of van der Waals and Platteeuw to represent the equilibrium formation of hydrates containing the considered guest molecules. The application of this theory generally requires parameters, referred to as Kihara parameters, that are influenced by the molecular properties as well as the reliability of experimental data. Meticulous consideration and caution are essential when selecting data to be utilized. Thus, the purpose of this paper is to analyse thermodynamic models that can resolve the equilibrium between guest molecules and the promoter, to attempt an identification of the thermodynamic equilibria, initially as pure components, and then to analyse the system using the hydrate model to be described later, paying particular attention to the results obtained.

1.1 Binary equilibrium modeling

The liquid–vapor equilibrium represents a fundamental condition for analyzing the coexistence behavior of the liquid and vapor phases of two or more components under equilibrium conditions. To understand its mechanisms, different thermodynamic models are employed depending on the components of the mixture. These models are capable of correlating various properties of the components (such as temperature, pressure, and compositions) through a series of mathematical steps suited to the purpose. This chapter will examine several models used for the objectives of this paper, starting with those useful for analyzing binary equilibria between the molecules considered. The models discussed are: SRK, PR, and PR78.

1.2 Soave-Redlich-Kwong (SRK) equation of state

The **Soave–Redlich–Kwong (SRK)** equation of state is a widely used cubic thermodynamic model for describing the behavior of liquid and vapor phases in non-ideal binary systems. The general form of the equation is[12]:

$$P = \frac{RT}{V_m - b} - \frac{a(T)}{V_m(V_m + b)} \tag{1.1}$$

- P is the system pressure
- T is the absolute temperature
- V_m is the molar volume
- R is the ideal gas constant
- $a(T)$ is the temperature-dependent attraction parameter
- b is the co-volume parameter

For a pure component i, the parameters $a_i(T)$ and b_i are defined as:

$$a_i(T) = 0.42748 \frac{R^2 T_{c,i}^2}{P_{c,i}} \alpha_i(T) \tag{1.2}$$

$$\alpha_i(T) = \left[1 + m_i \left(1 - \sqrt{\frac{T}{T_{c,i}}}\right)\right]^2 \tag{1.3}$$

$$m_i = 0.480 + 1.574\omega_i - 0.176\omega_i^2 \tag{1.4}$$

$$b_i = 0.08664 \frac{RT_{c,i}}{P_{c,i}} \tag{1.5}$$

- $T_{c,i}$ is the critical temperature of component i
- $P_{c,i}$ is the critical pressure of component i
- ω_i is the acentric factor of component i

For a binary mixture, the parameters a and b are combined using mixing rules:

$$a = \sum_{i=1}^{2} \sum_{j=1}^{2} x_i x_j a_{ij} \tag{1.6}$$

$$a_{ij} = \sqrt{a_i a_j}(1 - k_{ij}) \tag{1.7}$$

$$b = \sum_{i=1}^{2} x_i b_i (1 - I_{ij}) \tag{1.8}$$

- x_i is the mole fraction of component i in the mixture
- k_{ij} is the binary interaction parameter, typically determined experimentally

Phase equilibrium between the liquid and vapor phases is achieved by equating the fugacities of each component in both phases:

$$\hat{f}_i^L = \hat{f}_i^V \quad \text{for} \quad i = 1{,}2 \tag{1.9}$$

The fugacity coefficient for a mixture ϕ_i is calculated as:

$$\ln \phi_i = \frac{b_i}{b}(Z - 1) - \ln(Z - B) + \frac{A}{B}\left(\frac{2\sum_{j=1}^{2} x_j a_{ij}}{a} - \frac{b_i}{b}\right) \ln\left(1 + \frac{B}{Z}\right) \tag{1.10}$$

- Z is the compressibility factor, obtained as a solution of the cubic equation derived from the equation of state
- $A = \frac{aP}{(RT)^2}$
- $B = \frac{bP}{RT}$

Several sources report slight variations in the formulation of the model, but the approach generally follows that of Chung-Tong Lin et al. (1978)[13]. Coefficients A and B reflect the presence of two phases and two components; when properly optimized, they help reduce the deviation between theoretical predictions and experimental results.. The expression for the fugacity coefficient in the SRK equation of state is adopted from Prausnitz et al. (1998)[14], which provides a comprehensive derivation and application of cubic equations of state for phase equilibrium calculations for a mixture.

1.3 Peng-Robinson Equation of State (PR)

Among the many cubic equations of state derived from the van der Waals model, the Peng-Robinson equation is widely used due to its simplicity and flexibility [15, 16, 17, 18]. The **Peng-Robinson** equation of state (PR) [19] represents an improvement over the SRK model and is particularly accurate in estimating liquid densities and phase equilibria for systems containing hydrocarbons and gases.

Furthermore, the Peng-Robinson equation was developed to better represent hydrocarbons with higher molecular weights, thus extending its applicability across a wider range of compounds and equilibrium conditions.

Its general form is:

$$P = \frac{RT}{V_m - b} - \frac{a(T)}{V_m(V_m + b) + b(V_m - b)} \tag{1.11}$$

The parameters $a_i(T)$ and b_i are defined as follows:

$$a_i(T) = 0.45724 \frac{R^2 T_{c,i}^2}{P_{c,i}} \alpha_i(T) \tag{1.12}$$

$$\alpha_i(T) = \left[1 + m_i \left(1 - \sqrt{\frac{T}{T_{c,i}}}\right)\right]^2 \tag{1.13}$$

$$m_i = 0.37464 + 1.54226\omega_i - 0.26992\omega_i^2 \quad (\omega_i \leq 0.49) \tag{1.14}$$

$$b_i = 0.07780 \frac{RT_{c,i}}{P_{c,i}} \tag{1.15}$$

For binary mixtures, the parameters are combined using:

$$a = \sum_{i=1}^{2} \sum_{j=1}^{2} x_i x_j (a_i a_j)^{0.5} (1 - k_{ij}) \tag{1.16}$$

$$b = \sum_{i=1}^{2} x_i b_i \tag{1.17}$$

The VLE condition requires the equality of fugacities:

$$\hat{f}_i^L = \hat{f}_i^V \tag{1.18}$$

The fugacity coefficient in the Peng–Robinson formulation is given by:

$$\begin{aligned}\ln\phi = & -\log(Z-B)+\frac{b_i}{b}\left(\frac{B}{Z-B}-\frac{AZ}{Z^2+2BZ-B^2}\right)- \\ & -\frac{A}{2^{3/2}B}\left(2\frac{(a_{ij}\mathbf{x}^\top)^\top}{a}-\frac{b_i}{b}\right) \quad \times\log\left(\frac{Z+2.4142B}{Z-0.4142B}\right)\end{aligned} \tag{1.19}$$

where $A = aP/(RT)^2$, $B = bP/RT$, e Z is the solution of the cubic equation:

$$Z^3-(1-B)Z^2+(A-2B-3B^2)Z-(AB-B^2-B^3)=0 \tag{1.20}$$

Binary interaction coefficients, as in the case of the SRK model, are evaluated experimentally and used to minimize the model error. However, in some cases experimental data may be unavailable, and thus these coefficients are set to zero. As can be observed, the two models mainly differ in the expression for the calculation of the fugacity coefficient, which is modified due to changes in the model formulation.

1.4 PR78 Variant: Enhancements to the Original Formulation

The 1978 revision [20] introduces critical modifications to the function $\alpha_i(T)$ for improved accuracy with heavy and polar components:

$$\alpha_i^{PR78}(T)=\left[1+m_i\left(1-\sqrt{\frac{T}{T_{c,i}}}\right)\right]^2 \tag{1.21}$$

The acentric factor correlation has been optimized:

$$m_i = 0.37464+1.54226\,\omega_i-0.26992\,\omega_i^2, \qquad \text{se } \omega_i\le 0.49, \tag{1.22}$$

$$m_i = 0.379642+1.48503\,\omega_i-0.164423\,\omega_i^2+0.016666\,\omega_i^3, \quad \text{se } \omega_i>0.49. \tag{1.23}$$

For mixtures containing polar components (e.g., water–hydrocarbons), PR78 suggests:

$$k_{ij}=-\frac{1}{2}\sum_{k=1}^{N_g}\sum_{l=1}^{N_g}(\alpha_{ik}-\alpha_{jk})(\alpha_{il}-\alpha_{jl})\cdot\frac{-A_{12}\left(\frac{298.15}{T}\right)^{\frac{A_{12}}{B_{1K}}-1}-\left(\frac{\sqrt{a_i}}{b_i}-\frac{\sqrt{a_j}}{b_j}\right)^2}{\frac{2\sqrt{a_ia_j}}{b_ib_j}} \quad \text{with} \quad k_{ii}=0 \tag{1.24}$$

The modified form for calculating the fugacity retains the structure of the Peng–Robinson equation but uses the new α_i^{PR78}:

$$\begin{aligned}\ln\phi = & -\log(Z-B)+\frac{b_i}{b}\left(\frac{B}{Z-B}-\frac{AZ}{Z^2+2BZ-B^2}\right)- \\ & -\frac{A}{2^{3/2}B}\left(2\frac{(a_{ij}\mathbf{x}^\top)^\top}{a}-\frac{b_i}{b}\right) \quad \times\log\left(\frac{Z+2.4142B}{Z-0.4142B}\right)\end{aligned} \tag{1.25}$$

As previously discussed by Jean-Noel Jaubert et al. [20], substantial modifications have been introduced in the calculation of binary interaction coefficients through the use of new constants, which were further detailed and analyzed by Romain Privat (2008)[21].For simplicity, the values α_{11} and α_{22} were set to zero to consider only the data at equilibrium and of the mixture. These values, A_{12} and B_{12}, will be reported later in the discussion of the final result of the equilibra. This work provides data for all binary equilibria among the components of the mixture under study: cyclopentane (CP), carbon dioxide (CO_2), and nitrogen (N_2). The following table reports all the data related to the components of the mixture in question, useful for the model calculations:

Table 1.1: Critical data and acentric factor for carbon dioxide, nitrogen and cyclopentane [22, 23]

Components	T_c **(K)**	P_c **(bar)**	ω
Cyclopentane	511.7	45.1	0.195
Nitrogen	126.2	34	0.0377
Carbon dioxide	304.21	73.83	0.224

After introducing the various models and providing all the necessary data for the numerical calculation of binary vapor-liquid equilibrium, we will proceed to a detailed analysis, examining the differences between the numerical models and the experimental data, as compared to the literature.

Chapter 2

Binary equilibrium

2.1 Cyclopentane

An interesting approach to the distillation process based on hydrate formation with guest molecules is to introduce a promoter in order to facilitate the creation of cages that can trap stable gas molecules. The objective remains to stabilize and recover both the guest molecules (CO_2, N_2) and the promoter, so that they can be reused.

Due to the technological challenges encountered, several promoters have been investigated by M. Aminnaji et al. [24], but in this work particular attention is given to the use of cyclopentane.

Cyclopentane (CP) is able to form hydrates with pure water between 6.3°C and 7.7°C, with minor deviations due to experimental procedures. In the desalination process, atmospheric pressure conditions are more favorable than either high-pressure or vacuum conditions [11]. Compared to other tested promoters, cyclopentane shows lower environmental impact.

At high pressures, Trueba et al. [25] conducted measurements on phase equilibria of structure II clathrate hydrates, demonstrating that the equilibrium temperature remains essentially independent of pressure, due to the low compressibility of the two fluid phases and the solid phase. This result suggests that, in the absence of gas molecules, the dissociation temperature of hydrate cyclopentane does not vary significantly with increasing pressure [25].

To further investigate the hydrate formation process, it is first necessary to study the binary chemical equilibria between the gas molecules and the promoter, and then compare experimental results with thermodynamic models, namely the Soave–Redlich–Kwong (SRK), Peng–Robinson (PR), and Peng–Robinson 78 (PR78) equations of state, to evaluate which best reproduces the observed data.

2.2 Carbon dioxide, nitrogen binary equilibrium

2.2.1 CO_2–N_2 VLE at 288K

The first binary equilibrium is represented between carbon dioxide and nitrogen, a complex system due to the characteristics of the two components, which makes the vapor-liquid equilibrium curves difficult to determine.

To provide a general overview of how the equilibrium varies and to ensure a detailed analysis of the differences between the models, three different equilibrium temperatures were analyzed at varying pressure. This allows the evaluation, in different cases, of which model among those studied is able to minimize the error in matching the theoretical curve with the experimental one, reported by Aleksander Kreglewski et al. [26].

The analyses were carried out at temperatures of 288.15 K, 273.15 K, and 218.18 K.

For the carbon dioxide (CO_2) and nitrogen (N_2) system, Figure 2.1 shows the theoretical and experimental curves at a constant temperature of 288.15 K.

The red dotted curve represents the results obtained from the simulation of the SKR model, the green dotted curve represents the Peng-Robinson 78 model, and the black curve represents the experimental data[27]. The results are as follows:

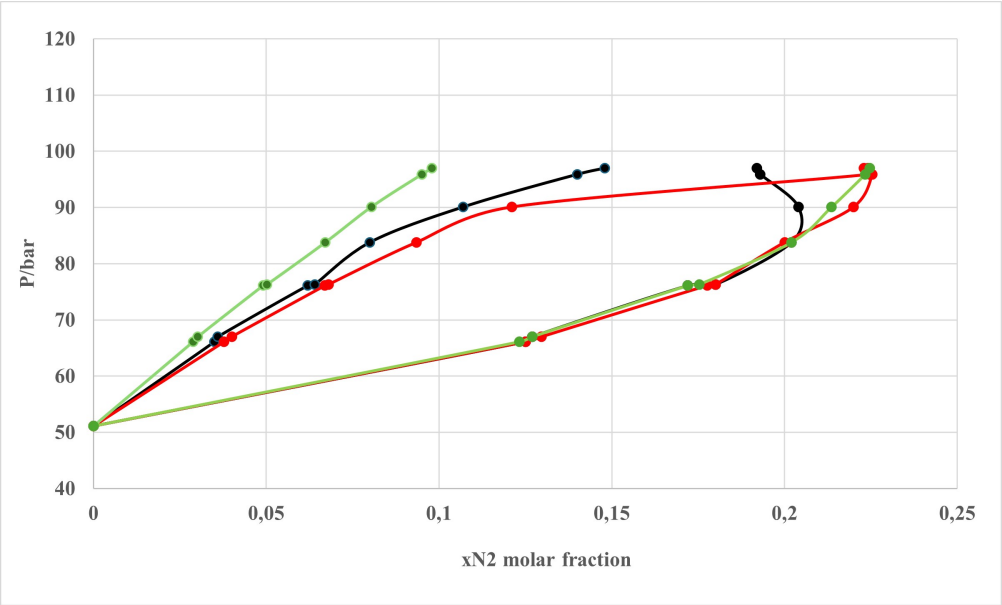

Figure 2.1: Comparison of experimental and theoretical data for the equilibrium of CO_2 + N_2 at a temperature of 288.3 K. The dotted black curve represents experimental data; the dotted red curve represents data from the SKR model ($k_{ij} = 0$); the dotted green curve represents data from the PPR78 model ($k_{ij} = 0.1101$).

For the SKR model, no binary interaction parameters are available in the literature; therefore, $k_{ij} = 0$ was assumed.

The Peng-Robinson model did not yield valid results for comparison, even when using the binary interaction coefficient reported by Jürgen Stoll et al. [27], namely $k_{ij} = -0.0149$.

For the PR78 model, the calculated binary interaction coefficient was $k_{ij} = 0.1101$. To simplify the calculations and focus solely on vapor-liquid interactions between the two components, the diagonal parameters were set as $k_{11} = 0$ and $k_{22} = 0$.

To compare the theoretical model data with the experimental results, the Absolute Deviation Data (ADD) was calculated for each model:

$$\text{ADD} = \frac{1}{N} \sum_{i=1}^{N} \left| y_i^{\text{exp}} - y_i^{\text{calc}} \right| \tag{2.1}$$

The ADD values are 0.0966 for the SKR model and 0.007 for the PR78 model, respectively.

Thus, both models approximate the trend of the experimental curve, reproducing the real behavior in the liquid phase with an error percentage of approximately 1%.

A notable observation is the low nitrogen concentration, which implies a higher carbon dioxide presence in the mixture. These low concentrations introduce various challenges in the calculation of equilibrium compositions.

2.2.2 CO_2–N_2 VLE at 273.15K

In Figure 2.2, the equilibrium data at a constant temperature of 273.15 K are reported.

The red dotted curve again represents the results obtained from the SKR model simulation, the green dotted curve corresponds to the Peng-Robinson 78 model, and the black curve represents the experimental data [26].

The results are as follows:

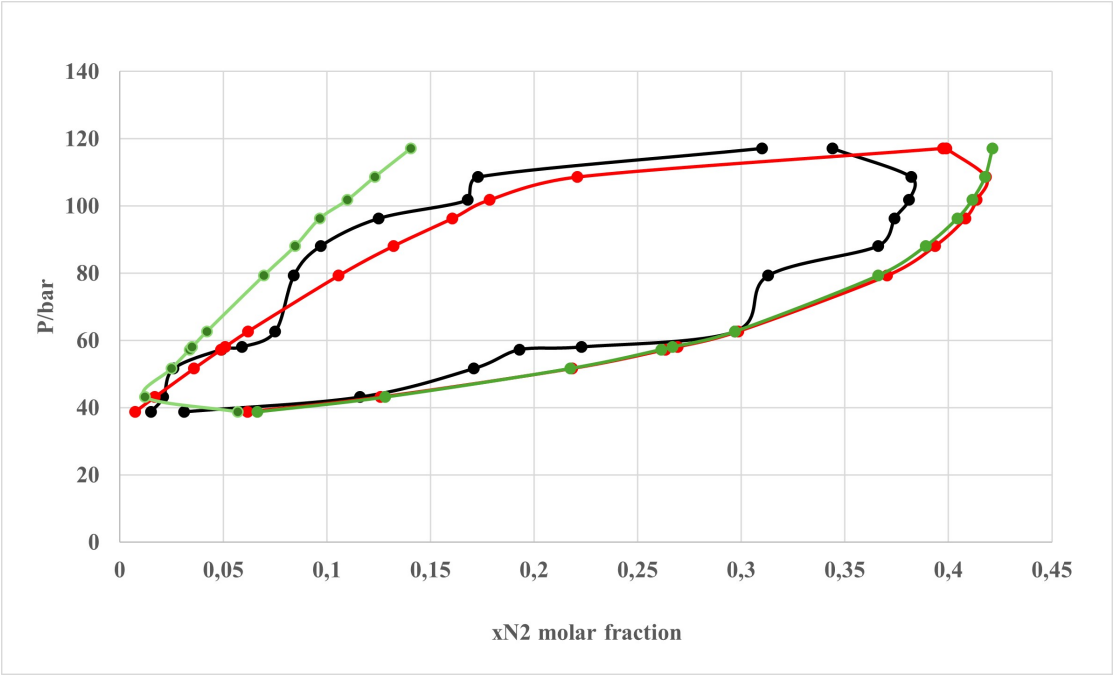

Figure 2.2: Comparison of experimental and theoretical data for the equilibrium of CO_2 + N_2 at a temperature of 273.15 K. The solid black curve represents experimental data; the dashed red curve represents data from the SKR model ($k_{ij} = 0$); the dashed green curve represents data from the PR78 model ($k_{ij} = 0.1104$).

The assumptions made for the SKR and PR78 models remain valid for the analyses at different temperatures.

For the P78 model, the calculated binary interaction coefficient is $k_{ij} = 0.1104$; for simplification purposes, $k_{11} = 0$ and $k_{22} = 0$ are assumed again.

To compare the theoretical model data with the experimental results, the maximum absolute deviation (ADD) was calculated for each model, with values of ADD = -0.037 for SKR and ADD = 0.038 for PR78, respectively.

Both models show similar ADD values and, from a computational perspective, exhibit the same level of error; however, by observing the trend of the curves, significant differences emerge.

The SKR model tends to overestimate the experimental data while following the same general trend. This discrepancy may be due to a lack of sufficient experimental data, which prevents an accurate curve fitting.

On the other hand, the PR78 model produces a denser curve, but it deviates from the experimental trend at higher pressures, corresponding to lower nitrogen concentrations.

Compared to the curves at 288.3 K, nitrogen concentrations have increased up to a maximum liquid concentration of $y_{N_2} = 0.42$, compared to $y_{N_2} = 0.22$ at just 15 K higher.

2.2.3 CO_2–N_2 VLE at 218.15K

In Figure 2.3, the equilibrium data at a constant temperature of 218.15 K are reported.

As before, the red dotted curve represents the results obtained from the SKR model simulation, the green dotted curve corresponds to the Peng-Robinson 78 model, and the black curve represents the experimental data [26].

The results are as follows:

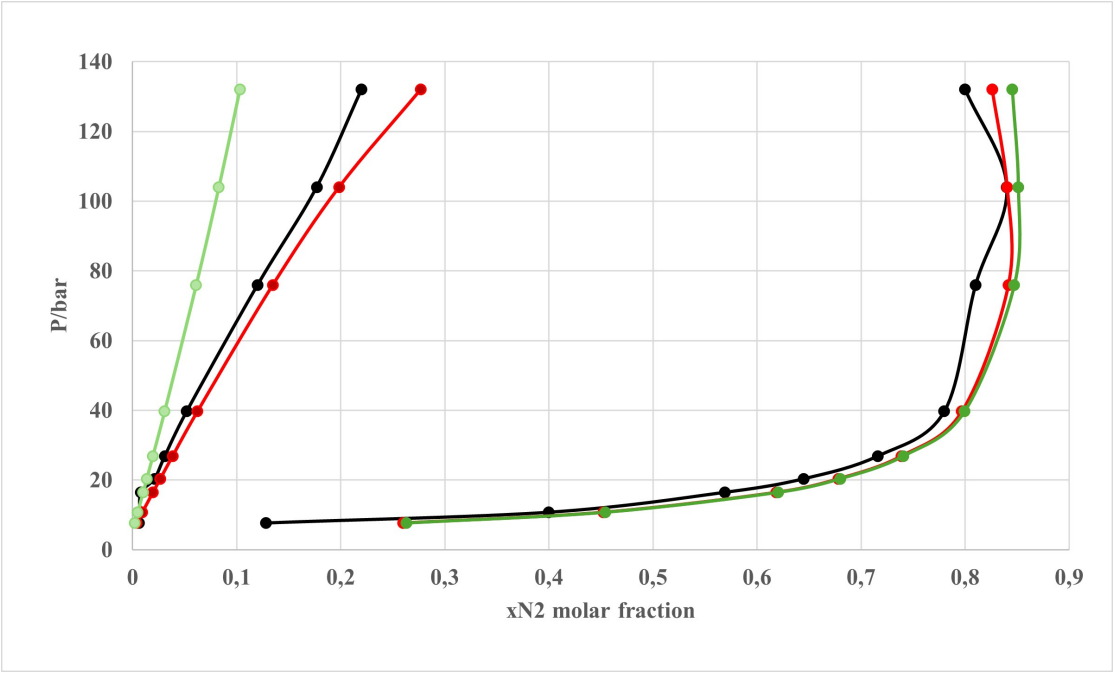

Figure 2.3: Comparison of experimental and theoretical data for the equilibrium of CO_2 + N_2 at a temperature of 218.15 K. The solid black curve represents experimental data; the dashed red curve represents data from the SKR model ($k_{ij} = 0$); the dashed green curve represents data from the PPR78 model ($k_{ij} = 0.1048$).

In the final analysis conducted for the vapor–liquid equilibrium between carbon dioxide and cyclopentane at a temperature of 218.3 K, the two equilibrium curves show different behaviors.

On the liquid side, the theoretical trend closely follows the experimental data, except for a higher nitrogen composition predicted by both models.In contrast, for the vapor phase curve, the two models show divergent behavior: the SKR model predicts a higher nitrogen concentration, while the Peng-Robinson 78 model, consistent with the previous analysis, shows a trend where the nitrogen mole fraction

decreases as pressure increases. Analyzing the absolute deviations of both models, the SKR model yields an ADD = 0.04 and the PR model an ADD = 0.046, both corresponding to an error of 4%, despite the different curve shapes. Once again, it is important to note that as temperature decreases, the nitrogen mole fraction significantly increases. Table 2.1 summarizes the main values obtained from the analyses carried out for the SKR, PR, and PR78 models at each specific temperature, including the corresponding binary interaction parameters and standard deviations.

Model	T (K)	P (bar)	K_{ij}	ADD_x	ADD_y
SKR	288.3	51.1–97	\	-0.023	-0.009
	273.3	38.8–117	\	-0.018	-0.037
	218.15	7.71–132	\	-0.014	-0.041
PR	288.3	51.1–97	\	\	\
	273.3	38.8–117	\	\	\
	218.15	7.71–132	\	\	\
PR78	288.3	51.1–97	0.1101	0.019	-0.007
	273.3	338.8–117	0.1104	0.031	-0.038
	218.15	7.71–132	0.1048	-0.045	-0.0458

Table 2.1: Data for modelling binary equilibrium CO_2+N_2.

2.3 Carbon dioxide, cyclopentane binary equilibrium

2.3.1 CO_2–CP VLE at 344.7K

The second equilibrium system considered is between carbon dioxide (CO_2) and cyclopentene (CP). The vapor-liquid equilibrium between the two components was experimentally studied by Nilesh N. Shah et al. [28], with temperatures ranging from 275 to 493 K. Among the available temperatures, three were selected: 344.7 K, 310.86 K, and 276.44 K. All three models will be analyzed, and to compare the binary interaction coefficients, the work of Sergiu Sima et al. [29] with the SKR and PR models is considered. For each model, at the corresponding system temperature, all values of the binary interaction coefficients are reported. In addition, the PR78 model is explored, and the differences between the respective equilibrium curves are analyzed. For each temperature, the graph will report the values of all the identified models, where the SKR model is represented by a red dotted line, the PR model by a blue dotted line, the PR78 model by a green dotted line, and finally, the experimental values are shown by a black line. Figure 2.4 shows the vapor-liquid equilibrium between carbon dioxide and cyclopentene at the temperature of 344.7 K, with a pressure range from 0 to 120 bar.

Starting from the red curve of the SKR model, the validity of the data is observed only up to a pressure of 45 bar, below which an ADD of 0.06 is obtained, following the experimental curve. As previously done for the former system, in this case as well we assume $k_{11} = 0$ and $k_{22} = 0$, an assumption that will also apply to the following equilibrium analyses.

For the calculation of the equilibrium, the binary interaction coefficients used were $k_{ij} = 0.1290$ and $I_{ij} = 0.030$ [28], which are not sufficient to reduce the calculation error at high pressures. A similar trend was obtained from the PR model, where the simulation also does not exceed 45 bar, using coefficients $k_{ij} = 0.1190$ and $I_{ij} = -0.0387$ [29]. The standard deviation measured for the PR model is ADD = 0.042, slightly lower than that of SKR, although it presents a different trend for the vapor phase compared to the experimental curve, diverging at higher pressures.

The PR78 model proves to be an excellent candidate for describing vapor-liquid equilibrium under these operating conditions, as it presents a complete behavior over the entire equilibrium pressure range. The binary interaction coefficient used is $k_{ij} = -0.032$, with the group interaction coefficients taken from [28]: $A_{kl} = 91.28$ and $B_{kl} = 82.01$. These values will also be valid for the subsequent analyses. The calculated line using this model shows significantly lower pressures, and the curve reflects the experimental behavior predicted by Aleksander reglewski [26].

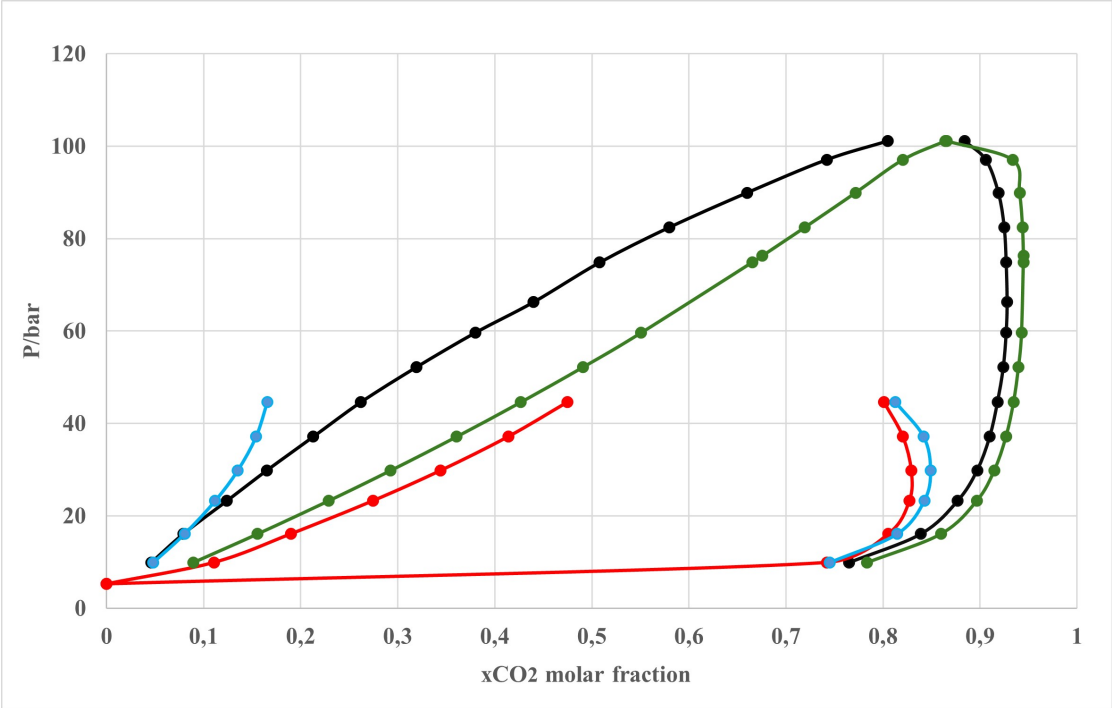

Figure 2.4: Comparison of experimental and theoretical data for the equilibrium of CO_2 + CP at a temperature of 344.7K; solid black curve represents experimental data ; the dotted red curve represents SKR model data (kij =0.1290, Iij=0.030);the dotted blue curve represents PR model data (kij=0.1190, IIJ=-0.0387); the dotted green curve represents PPR78 model data (kij =-0.032).

2.3.2 CO_2–CP VLE at 310.K

The second comparison between models and experimental data was carried out at a temperature of 310.8 K, with a pressure range from 0 to 65 bar. In figure 2.5, the equilibrium curves of the various models are shown, with the attempt by Aleksander Kreglewski [26] represented by the black curve.

From the graph, the absence of the SKR model can be observed. Even with the use of binary interaction parameters ($k_{ij} = 0.1290$, $I_{ij} = 0.030$) aimed at reducing the calculation error, the model fails to return usable data for interpreting the vapor-liquid equilibrium.

The curve corresponding to the PR model, as in the previous case, is unable to exceed a pressure of 45 bar and diverges from the experimental trend. The gas phase is significantly deviated from the experimental curve, showing higher pressures with increased concentrations of carbon dioxide.

In contrast, the curve related to the PR78 model shows a trend that diverges

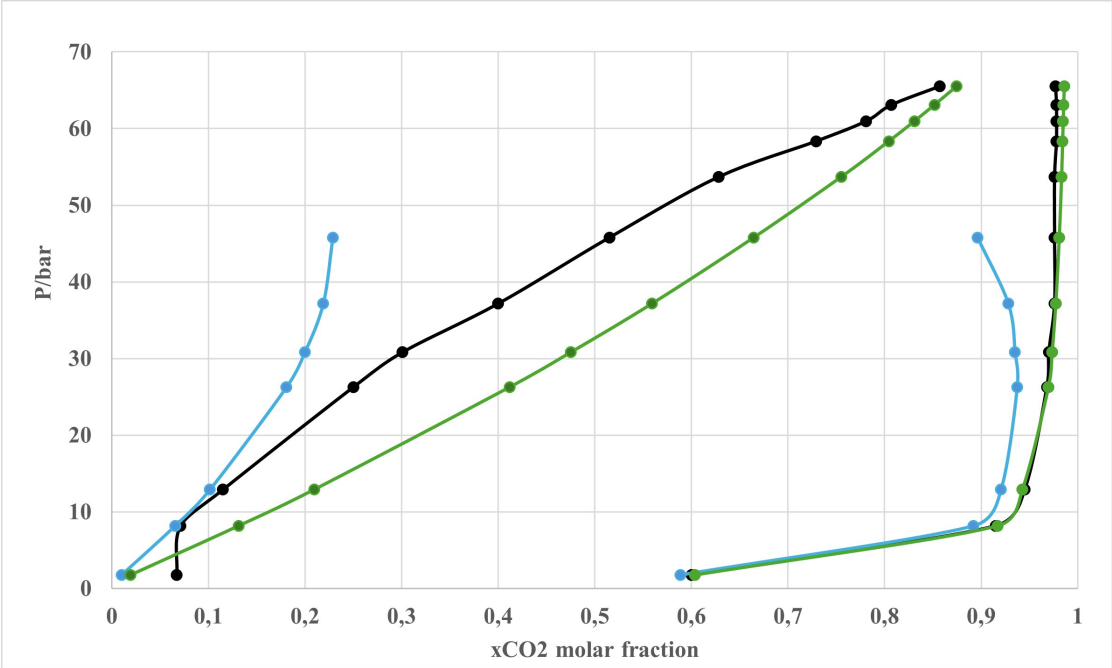

Figure 2.5: Comparison of experimental and theoretical data for the equilibrium of CO_2 + CP at a temperature of 310.0K; solid black curve represents experimental data the dotted blue curve represents PR model data (kij=0.1190, IIJ=-0.0387); the dotted green curve represents PPR78 model data (kij =-0.0026).

from the proposed model but matches the experimental curve, as confirmed by previous studies [28, 29]. The calculation of the binary interaction coefficient resulted in a value of -0.0026, which differs from those previously reported in the literature, but proves to be optimal for representing the model.

The PR78 model yields an ADD of 0.009, i.e., a deviation below 1%, lower than that of the PR model, which shows an ADD of 0.02. A reduction in the pressure range is observed with decreasing temperature, while the concentrations maintain the same trend, with the liquid phase of carbon dioxide prevailing even at low pressures.

2.3.3 CO_2–CP VLE at 276.6.K

Finally, the last attempt was made at a temperature of 276.64 K, and, as previously observed, the SKR model was again unable to provide values for this equilibrium system. In Figure 2.6 , the following data are presented: In the final attempt to best simulate the experimental data, at a temperature of 276.6 K, the curves once again show a trend that diverges from the experimental curve.

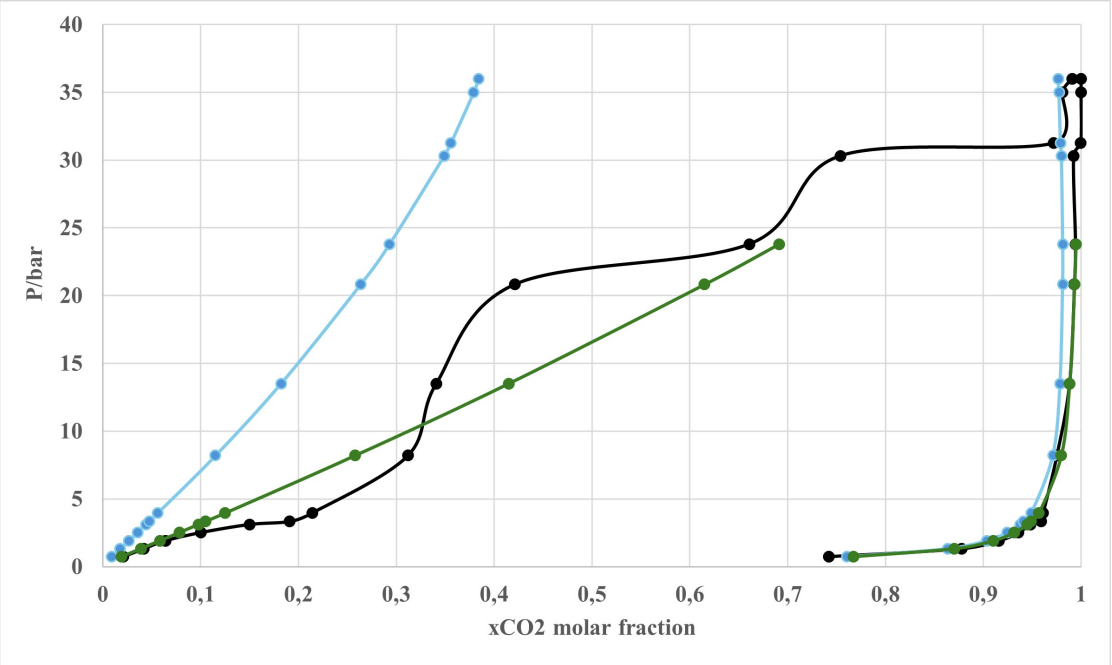

Figure 2.6: Comparison of experimental and theoretical data for the equilibrium of CP + CO_2 at a temperature of 276.6K; solid black curve represents experimental data the dashed blue curve represents PR model data (kij=0.1190, IIJ=-0.0387); the dashed green curve represents PPR78 model data (kij =-0.0006).

As a first analysis, the PR model shows a trend for the vapor phase that diverges toward higher pressures, with significantly lower concentrations compared to the experimental curve. This behavior could be due to interpolation using the binary interaction coefficients $k_{ij} = 0.1190$, $I_{ij} = -0.0387$ [29].

For the PR78 model, using the same group interaction coefficients [28], a binary interaction coefficient of $k_{ij} = -0.0006$ was found. The error is therefore below 1%, but the interactions stop providing reliable data starting from 24 bar, although up to that pressure the trend reflects the experimental curve.

Table 3 summarizes the main results of the analyses conducted for the SKR, PR, and PR78 models at each specific temperature, including the corresponding binary interaction parameters and standard deviations.

Model	T (K)	P (bar)	K_{ij}	I_{ij}	ADD_x	ADD_y
SKR	344.7	9–101	0.129	0.03	\	\
	310.86	0–35	0.129	0.03	\	\
	276.64	1–65	0.129	0.03	-0.153	0.063
PR	344.7	9–101	0.119	-0.038	0.0277	0.0428571
	310.86	0–35	0.119	-0.038	0.1020857	0.036
	276.64	1–65	0.119	-0.038	0.522	0.025
PR78	344.7	9–101	-0.032	\	0.019	-0.007
	310.86	0–35	-0.002	\	0.031	-0.038
	276.64	1–65	-0.006	\	-0.045	-0.045

Table 2.2: Data for modelling binary equilibrium CO_2+CP.

2.4 Nitrogen, cyclopentane binary equilibrium

2.4.1 N_2–CP VLE at 410.2K

The third and final equilibrium system analyzed involves nitrogen (N_2) and cyclopentene (CP), a stable mixture that is difficult to handle due to the high temperatures required to reach pressures comparable to the operative conditions considered. The vapor–liquid equilibrium (VLE) between these two components was experimentally investigated by Pradeep Marathe [30]. The VLE is valid over a pressure range up to 180 bar, and from the experimental data, the temperatures of 366.4 K and 410.2 K are considered. Due to the lack of available data, no binary interaction coefficients are reported for the SKR model. However, for the Peng–Robinson model, a temperature-dependent binary interaction coefficient is available: at 366.4 K, $k_{ij} = 0.01$, and at 410.2 K, $k_{ij} = 0.047$. At a temperature of 366.4 K, Figure 2.7 presents the results of the various models, following the previously established color scheme:

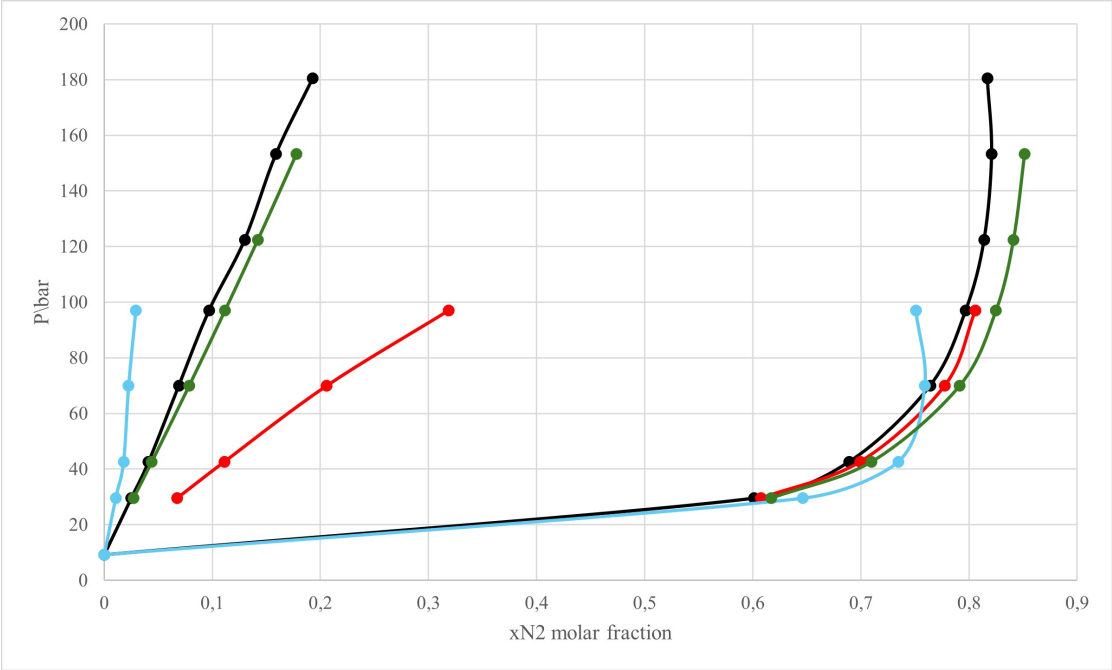

Figure 2.7: Comparison of experimental and theoretical data for the equilibrium of N_2 + CP at a temperature of 410.2K; solid black curve represents experimental data; the dashed red curve represents SKR model data the dashed blue curve represents PR model data (kij=0.047); the dashed green curve represents PPR78 model data (kij =0.1048).

By analyzing the behavior of the curves, a discrepancy can be observed across all models, with the Peng–Robinson 78 (PR78) model showing a trend comparable to the experimental curve. With group interaction values of $A_{ij} = 100.9$ and $B_{ij} = 249.8$ [31], and a binary interaction coefficient $k_{ij} = 0.1048$, the PR78 model is able to closely follow the experimental equilibrium curve, showing a slight deviation toward higher nitrogen molar concentrations in the vapor phase curve. Indeed, both the vapor and liquid curves exhibit a standard deviation of less than 1%.

In contrast, the SKR and PR models display divergent behavior: the SKR model yields a nearly linear liquid curve, but it significantly deviates from the experimental one, with an ADD_x of 0.13. The PR model, while also showing a linear trend, predicts considerably lower concentrations at the same pressure values.

On the vapor side, the SKR model fails to reproduce the equilibrium behavior, diverging completely from the experimental curve. In contrast, the PR model—with an ADD of 0.004—follows the experimental vapor trend more accurately.

As can be observed, some models are unable to complete the simulation,

terminating prematurely at lower pressures.

2.4.2 N_2–CP VLE at 366.4K

The final analysis presented in this work refers to the system at 366.4 K, which is lower than the previous attempt. As observed before, some models fail to complete the simulation and are unable to trace the entire equilibrium curve. Figure 2.8 shows the results, maintaining the same color scheme as previously used:

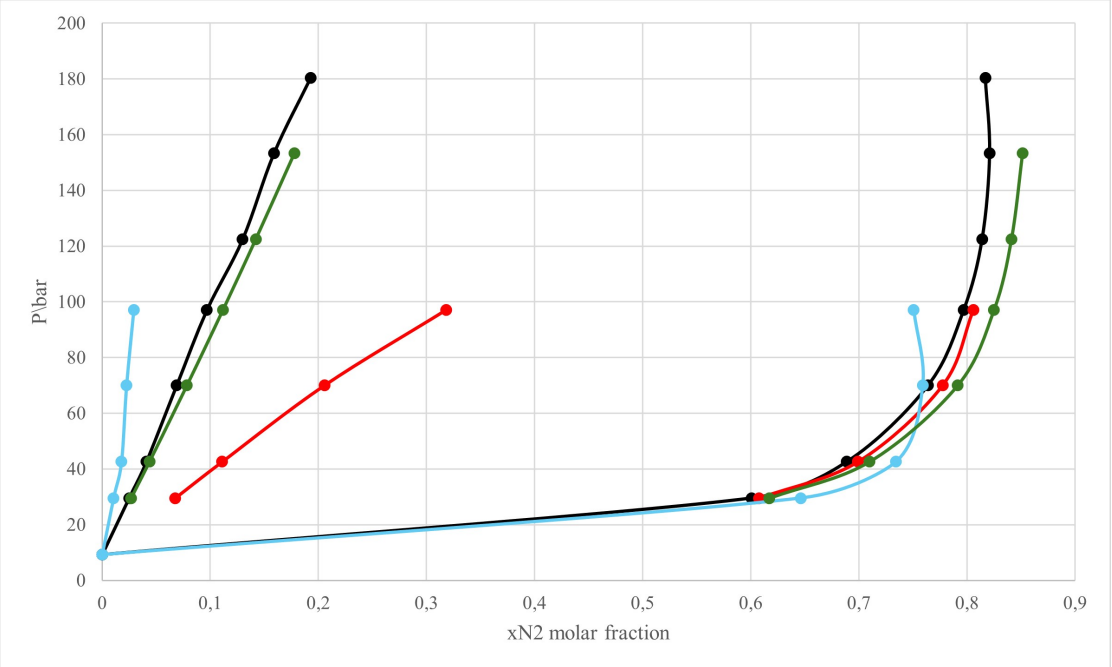

Figure 2.8: Comparison of experimental and theoretical data for the equilibrium of N_2 + CP at a temperature of 366.4K ; solid black curve represents experimental data; the daotted red curve represents SKR model data the dotted blue curve represents PR model data (kij=0.01); the dotted green curve represents PPR78 model data (kij =0.1048).

In the final attempt, the experimental curve is accurately reproduced only by the PR78 model, which with a binary interaction coefficient $k_{ij} = 0.01$ significantly reduces the error, keeping it below 1%. The only notable deviation is found in the vapor-phase curve, which shifts slightly toward higher concentrations as pressure increases, compared to the experimental curve.

As for the other two models, neither calculation provides results beyond 100 bar. The PR model fails to follow the equilibrium trend on both the liquid and vapor

sides. In contrast, the SKR model maintains an acceptable error on the vapor side, but the liquid-phase curve shows a trend that diverges from the experimental data.

Table 4 summarizes the main values obtained from the analyses carried out for the SKR, PR, and PR78 models at each specific temperature, including the corresponding binary interaction parameters and standard deviations.

Model	T (K)	P (bar)	k_{ij}	ADD_x	ADD_y
SKR	410.2	9.21–180.45	\	0.047	0.00395
	366.4	13.2–178.17	\	0.137	0.007
PR	410.2	9.21–180.45	0.047	-0.015	0.004
	366.4	13.2–178.17	0.01	-0.003	-0.028
PR78	410.2	9.21–180.45	0.1048	0.006	0.009
	366.4	13.2–178.17	0.093	-0.0001	0.023

Table 2.3: Data for modelling binary equilibrium N_2+CP.

In summary, after discussing the three main analytical methods employed SKR, PR, and PR78 reliable results for all equilibria are ensured only by the latter. The SKR and PR models, having binary coefficients independent of temperature, cannot provide reliable results for every equilibrium when considering different operating temperatures. Focusing instead on pressure ranges, both models behave similarly, namely that as pressure increases, the simulations struggle to follow the experimental trend.

Conversely, unlike the first two, thanks to the modifications introduced in the Peng–Robinson model with the PR78 formulation, by changing the calculation of the binary coefficient, it is possible to simulate all the analyzed equilibria at different pressure and temperature ranges. Moreover, in almost all cases, the model shows a lower standard absolute deviation. Therefore, for the continuation of the analysis where chemical equilibria between the same molecules will be examined during the formation of clathrate gases—the PR78 model will be used to extrapolate the fugacity coefficient for each individual mixture, necessary for the calculations.

Chapter 3

Hydrate Phase Equilibria: Theory and Modeling

Clathrate hydrates (or simply hydrates) are crystalline structures consisting of water molecules linked by hydrogen bonds that form cavities in which gas molecules or apolar compounds can be hosted. Among the most relevant applications of hydrates are gas storage, selective separation of mixtures, CO_2 capture and, more recently, desalination and water treatment processes.

In the case of apolar and poorly water-soluble guests such as cyclopentane, the interaction between the guest molecule and the water cavity can stabilize the formation of the hydrate phase even at atmospheric pressure, provided the temperature is sufficiently low. This phenomenon makes cyclopentane a thermodynamic promoter, capable of facilitating the formation of clathrates even in the presence of gases less prone to crystallize, such as nitrogen.

The theoretical description of these phenomena requires a model capable of accounting for:

- the fractional occupancy of cavities (there is no fixed stoichiometry),
- the molecular interaction between guest and water lattice,
- the contribution of water activity, especially in the presence of salts or organic promoters.

For this reason, the present work adopted the statistical–thermodynamic model of Platteeuw and van der Waals, which makes it possible to describe the chemical potential of water in the hydrate phase as a function of:

- temperature and pressure,
- the fugacity of the guest component,

- the guest–cavity interaction parameters (modeled through the Kihara potential),
- and the geometric structure of the lattice (typically SII in the case of cyclopentane).

Based on this theoretical framework, three systems were studied:

- CO_2/N_2, for which comparable experimental data are available,
- CO_2/cyclopentane (CP) and N_2/cyclopentane (CP), for which theoretical equilibrium (P–T) curves could be calculated, although data on the molecular compositions of the clathrates are lacking.

The following section will focus on the application of the model to these systems, presenting the results obtained, the limitations encountered, and the implications for the design of future experiments.

3.1 Van der Waals–Platteeuw Statistical Thermodynamic Model

In the thermodynamic equilibrium, the equality of chemical potential of water in the hydrate phase and liquid phase can be written by introducing reference states. For the hydrate, the reference state is a hypothetical phase β written by the van der Waals and Platteeuw model corresponding to the empty cavities:

$$\Delta\mu_w^{\beta-H} = \Delta\mu_w^{\beta-L} \tag{3.1}$$

where $\Delta\mu_w^{\beta-H}$ and $\Delta\mu_w^{\beta-L}$ are the differences of the chemical potentials between water in the reference phase (β) and water in the hydrate or liquid phase, respectively.

While $\Delta\mu_w^{\beta-L}$ can be expressed using the Gibbs-Duhem equation [32], $\Delta\mu_w^{\beta-H}$ is calculated from statistical Thermodynamics, from van der Waals and Platteeuw method:

$$\Delta\mu_W^{\beta-H} = -RT\sum_i v_i \ln\left(1 - \sum_j \theta_j^i\right) \tag{3.2}$$

where R is the universal constant, T is the absolute temperature, v_i is the number of type i cavities per water molecule in the hydrate (8/136 for CPH), and θ_j^i is the occupancy factor ($\theta_j^i \in [0,1]$) of the cavities of type i by the guest molecule j (the guest molecule here is CP). θ_j^i can be written by the Langmuir adsorption model and is expressed as follows:

$$\theta_j^i = \frac{C_j^i f_j(T,P)}{1+\sum_j C_j^i f_j(T,P)} \tag{3.3}$$

where f_j is the fugacity of the guest j (CP). C_j^i is the Langmuir constant of guest j in cavity i. It is usual to obtain C_j^i from the integration of the Kihara interaction potential as follows:

$$C_j^i = \frac{4\pi}{kT}\int_0^{R-a} \exp\left(\frac{-w(r)}{kT}\right) r^2 dr \tag{3.4}$$

where k is the Boltzmann constant, r is the distance from the center of the cavity, R is the empty cavity radius, $w(r)$ is the interaction potential between the cavity and the guest molecule, and a is the core radius defined in the Kihara potential. The interaction potential $w(r)$ is determined by the Parrish and Prausnitz model [33] and can be expressed as follows:

$$w(r) = 2ze\left[\frac{\sigma^{12}}{R^{11}r}\left(\delta^{10}+\frac{a}{R}\delta^{11}\right) - \frac{\sigma^6}{R^5 r}\left(\delta^4+\frac{a}{R}\delta^5\right)\right] \tag{3.5}$$

$$\delta^N = \frac{1}{N}\left[\left(1-\frac{r}{R}-\frac{a}{R}\right)^{-N} - \left(1+\frac{r}{R}-\frac{a}{R}\right)^{-N}\right] \tag{3.6}$$

Parameters ε, σ, a are so-called Kihara parameters. ε corresponds to the maximum attractive potential and σ is the distance between the cores at zero potential energy. They can be calculated from experimental data by fitting the model equations to correspond the equilibrium experimental one [**hassefiere2013**, 34, 35, 36, 37]. In this description, the interaction potential is dependent only on the properties of the guest molecule (via Kihara parameters), and the geometrical properties of the cavities (via the coordination number z and radius R).

In the end, both chemical potentials are function of the temperature and the salt concentration. On the one hand, in the liquid part, the pressure is atmospheric, and does not affect the equilibrium significantly. Only the temperature and the water activity (hence the salt concentration) are the major variables. Of course, property parameters are needed. Working with the parameters from Handa and Tse [38] after verifying they correspond the best [39].

On the other hand, the hydrate potential is a function of the CP fugacity, since the Kihara parameters are constant for a given guest. CP fugacity should be the same in all phases: liquid, hydrate and vapor. Since liquid CP can be considered as a pure phase (very low solubility of water in CP), fugacity was calculated from its vapor pressure. Therefore, a standard Antoine's equation was used, assuming that $f_{CP} = P_{CP}^{sat}$ (f_{CP} and P_{CP}^{sat} being the fugacity and the saturated pressure of CP, respectively). This fugacity is only temperature dependent.The calculation of

the temperature from a given salt concentration, or the opposite, can be obtained from the van der Waals equation.

The value of a was determined based on the method described by Tee et al.[40] The values of $\Delta\mu_w^{L-\beta}|_{T^0,P^0}$, $\Delta h_w^{L-\beta}|_{T^0,P^0}$, $b_{P,w}^{L-\beta}$, $\Delta C_{P,w}^{L-\beta}|_{T^0,P^0}$, and $\Delta v_w^{L-\beta}|_{T^0}$ can be found in the literature detailed in Table 3 and 4 as cited by Sloan.[41, 42]

Table 3.1: Parameters used for the hydrate-phase and ice (for Hydrate Structure II only).[38]

$\Delta\mu_w^{\beta-L}\|_{T_0,P_0}$ (J/mol)	$\Delta h_w^{\beta-I}\|_{T_0,P_0}$ (J/mol)
1068	-5247

Table 3.2: Reference properties of hydrate (for Hydrate Structure II only).[43]

Parameter	**Unit**	**Value**
$\Delta V^{\beta-L}\|_{T_0,P_0}$	$m^3 \cdot mol^{-1}$	4.9944×10^{-6}
$\Delta C_{p,w}^{\beta-L}\|_{T_0,P_0}$	$J \cdot mol^{-1} \cdot K^{-1}$	-38.12
β^L	$J \cdot mol^{-1} \cdot K^{-2}$	0.141
P_0	MPa	0

For a given set of Kihara parameters ε_j, σ_j and a given experimental temperature was calculated the interaction potential $w(r)$ in Eq.(3.5), the Langmuir constant C_j^i in Eq.(3.4), and then $\Delta\mu_w^{\beta-H}$ in Eq.(3.2). The predicted-equilibrium temperature T_{pred} at the simulated concentration corresponds to the value at which $\Delta\mu_w^{\beta-H} = \Delta\mu_w^{\beta-L}$. In this way, it is possible to determine temperature–pressure curves, also varying the concentration, by using binary equilibrium calculations (both for the fugacity calculation and for the composition variation).

Below are the values of the Kihara parameters suggested by [39, 44]:

Table 3.3: Kihara potential parameters for the considered guest molecules

Molecule	σ [Å]	ϵ/k_B [K]	a [Å]
CO_2	2.968	169.09	0.680
N_2	3.022	127.40	0.3526
Cyclopentane	2.72	265.5	0.8968

The subsequent studies of the equilibria follow, with some systems being successfully optimized, while for others, either due to a lack of experimental data or unsuccessful calculations, it was not possible to trace comparable curves.

3.1.1 Clathrate equilibrium N_2–CO_2

In the following, the results of the simulations on the N_2–CO_2 system with clathrate formation are presented. The analyses were carried out by comparing the results obtained by Jean-Michel Herri *et al.* [45], which are summarized in Table 3.4 .

The experimental results were obtained at the same temperature in order to compare the hydrate mole fractions with the initial mole fractions of the pure components, after exposure to the corresponding hydrate formation process.

Based on the simulations performed, and using the Kihara parameters introduced earlier, it is possible to observe how the mole compositions vary with increasing pressure while keeping the temperature constant. Three separate analyses were conducted at 274 K, 277 K, and 280 K, respectively, showing a trend consistent with the literature data.

The graphs corresponding to the simulations at the different temperatures are reported in Figures 3 below.

Table 3.4: Comparison of experimental and simulated hydrate molar fractions of carbon dioxide and nitrogen equilibrium at different temperatures and pressures.

T (°C)	**P (MPa)**	**Exp. CO_2**	**Exp. N_2**	**Sim. CO_2**	**Sim. N_2**
0.85	1.39	1.00	0.00	1.00	0.00
0.85	1.77	0.99	0.02	0.97	0.03
0.85	2.35	0.95	0.05	0.91	0.09
0.85	2.84	0.93	0.07	0.87	0.13
0.85	3.46	0.90	0.10	0.82	0.18
0.85	7.24	0.58	0.42	0.66	0.34
0.85	11.20	0.34	0.66	0.50	0.50
0.85	14.93	0.18	0.82	0.29	0.71
0.85	17.93	0.00	1.00	0.00	1.00
3.85	1.95	1.00	0.00	1.00	0.00
3.85	2.60	0.98	0.02	0.97	0.03
3.85	3.38	0.95	0.05	0.89	0.11
3.85	5.23	0.89	0.11	0.90	0.10
3.85	11.98	0.54	0.46	0.58	0.42
3.85	15.50	0.35	0.65	0.46	0.54
3.85	19.17	0.19	0.81	0.31	0.69
3.85	24.04	0.00	1.00	0.00	1.00
6.85	2.80	1.00	0.00	1.00	0.00
6.85	3.60	0.98	0.02	0.96	0.04
6.85	4.23	0.96	0.04	0.92	0.08
6.85	5.07	0.94	0.06	0.88	0.12
6.85	8.28	0.86	0.14	0.77	0.23
6.85	14.97	0.64	0.36	0.64	0.36
6.85	20.75	0.45	0.55	0.52	0.48
6.85	26.69	0.22	0.78	0.34	0.66
6.85	32.31	0.00	1.00	0.00	1.00

Analyzing the molar compositions, a similar trend can be observed for all simulations, though with a deviation from the experimentally obtained compositions.

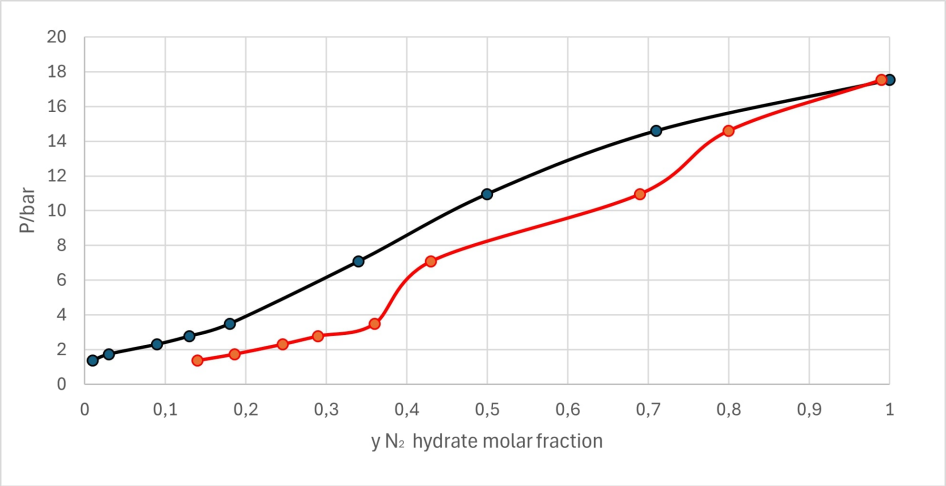

Figure 3.1: Comparison between experimental and simulated results for the hydrate molar fraction of N_2 in the CO_2–N_2 system at 274 K. Pressure is plotted as a function of the hydrate mole fraction of N_2.

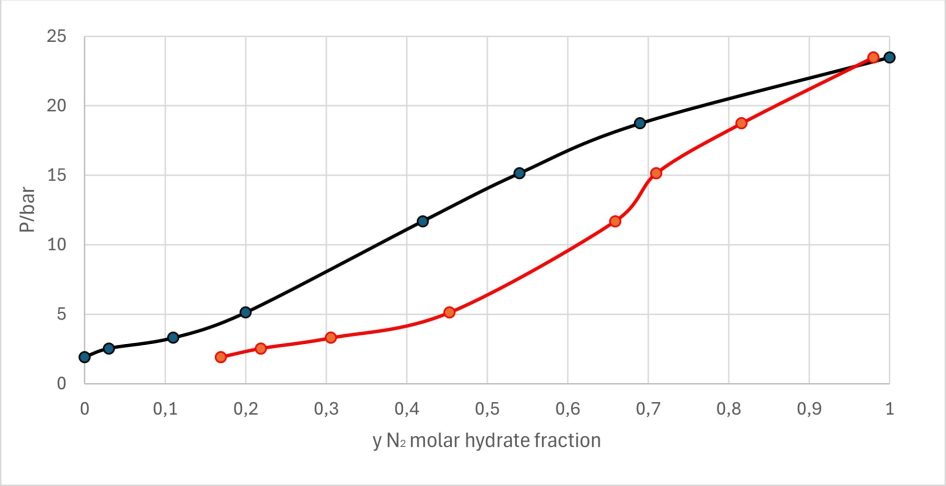

Figure 3.2: Comparison between experimental and simulated results for the hydrate molar fraction of N_2 in the CO_2–N_2 system at 277 K. Pressure is plotted as a function of the hydrate mole fraction of N_2.

At lower pressures, the presence of the gaseous hydrate phase of nitrogen is greater than the experimental result, with ADD values of 0.12, 0.146, and 0.171, respectively. From this, it can be deduced that the structure formed during hydrate formation contains higher amounts of nitrogen, but in practice, the system, with the previously determined Kihara parameters, may need slight adjustments to reduce the observed

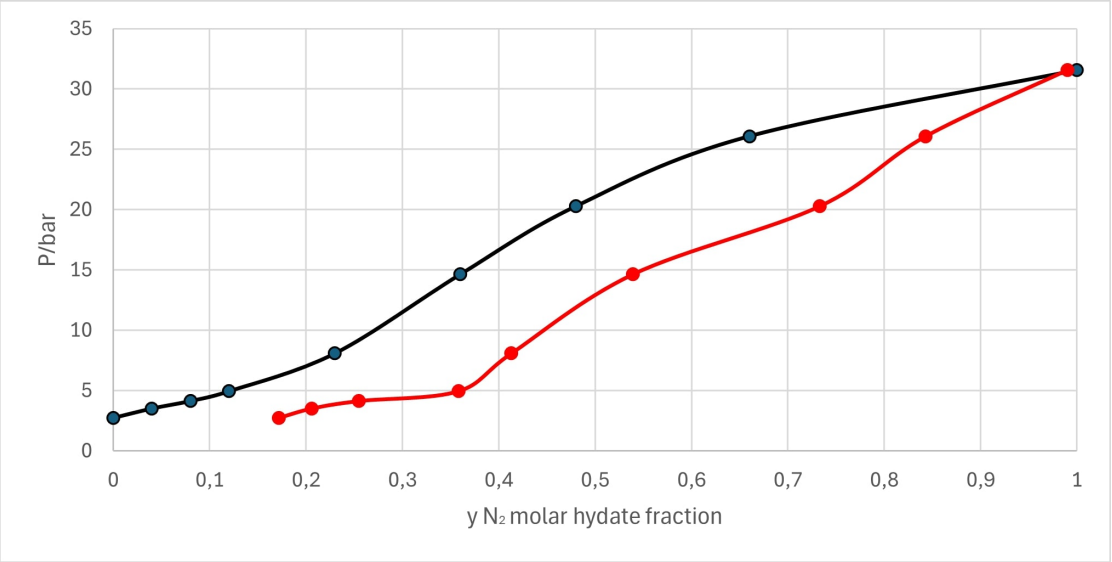

Figure 3.3: Comparison between experimental and simulated results for the hydrate molar fraction of N_2 in the CO_2–N_2 system at 280 K. Pressure is plotted as a function of the hydrate mole fraction of N_2.

standard deviation. For this analysis, the variation of molar compositions in the gaseous hydrate phase was examined, allowing an understanding of how the system changes with varying pressure while keeping the temperature fixed. Unfortunately, due to the limited availability of experimental data, a comparison between the temperatures predicted by the system and those observed during the experiments was not carried out.

3.1.2 Clathrate equilibrium CO_2-CP

Proceeding with the analysis of the different chemical equilibria during clathrate formation, we analyze the system of cyclopentane and carbon dioxide. This system has already been investigated in several studies, providing excellent experimental data from J. Zhang *et al.* [46]. The system is valid at temperatures ranging from 285.1 to 292.2 K and at relatively low pressures between 0.6 and 3.82 MPa. In relation to the previous analysis, we aim to determine, using the van der Waals and Platteeuw model, the temperature at which the system exhibits the equilibrium compositions between the gas components and the hydrate phase. Below, in Figure 3.4, the temperature trend with increasing pressure is shown.

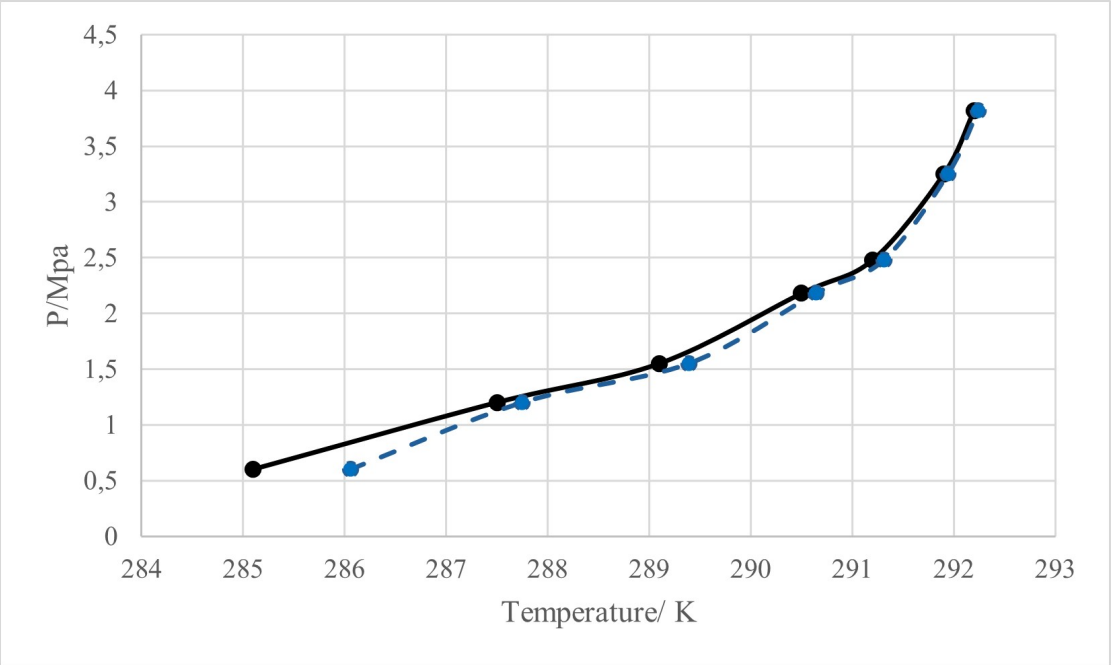

Figure 3.4: Temperature trend of the CP–CO_2 system with increasing pressure, based on the van der Waals and Platteeuw model.

It can be said that the theoretical trend is comparable to the experiments conducted; indeed, the two curves tend to overlap, presenting an ADD equal to 0.009, which is practically less than 1%. Regarding the compositions in this case, using the binary equilibrium, there appears to be a high gas-phase component of carbon dioxide, with a subsequent decrease in the gas-phase cyclopentane as the considered pressures increase. It is possible that the system is already stable and that the equilibrium between carbon dioxide and cyclopentane occurs with only a minimal presence of cyclopentane.

Table 3.5: Predicted temperatures and mole fractions in the hydrate phase for cyclopentane (CP) and carbon dioxide (CO_2).

$\mathbf{T_{pred}}$ **(K)**	$\mathbf{x}_{\mathbf{CP}}^{hydrate}$	$\mathbf{x}_{\mathbf{CO_2}}^{hydrate}$
286.06	0.03546	0.96454
287.75	0.01531	0.98469
289.39	0.01301	0.98699
290.64	0.00791	0.99209
291.31	0.00692	0.99308
291.94	0.00496	0.99504
292.24	0.00514	0.99486

3.1.3 Clathrate equilibrium N_2-CP

The hydrate phase equilibrium analyzed between cyclopentane and nitrogen is the most complex system, which, thanks to the use of the adopted binary coefficients, the Van der Waals and Platteuw hydrate model, and the suitable Kihara parameters, has been represented in Figure 3.5 showing the difference between experimental and theoretical equilibrium data as the system conditions vary.

In Figure 3.5, the continuous black curve represents the experimental data obtained from the literature, while the dashed blue curve represents the theoretical simulation of the hydrate model, which proves to be comparable. In fact, for this equilibrium a percentage standard deviation equal to 0.14% is obtained. Furthermore, it can be stated that cyclopentane, with excellent promoter performance, stabilizes the equilibrium, appearing with low mole fraction values that decrease as temperature and pressure increase.

To illustrate the effect of cyclopentane on both equilibria, Figure 3.6 shows the behavior of both equilibrium curves.

The graph shown in Figure 3.6 highlights the comparison between the hydrate formation curves for the CO_2–Cp and N_2–Cp systems. It can be observed that the black dashed curve, corresponding to the CO_2–Cp system, exhibits higher equilibrium pressures compared to the N_2–Cp system, indicated by the blue symbols with a solid black line. This result suggests that carbon dioxide, in the presence of cyclopentane, has a greater tendency to stabilize the equilibrium than nitrogen, which instead requires less extreme pressure and temperature conditions for hydrate formation. The comparison thus highlights the promoting effect of cyclopentane, which is more pronounced in the CO_2-containing system, making it potentially more suitable for carbon capture and storage applications.

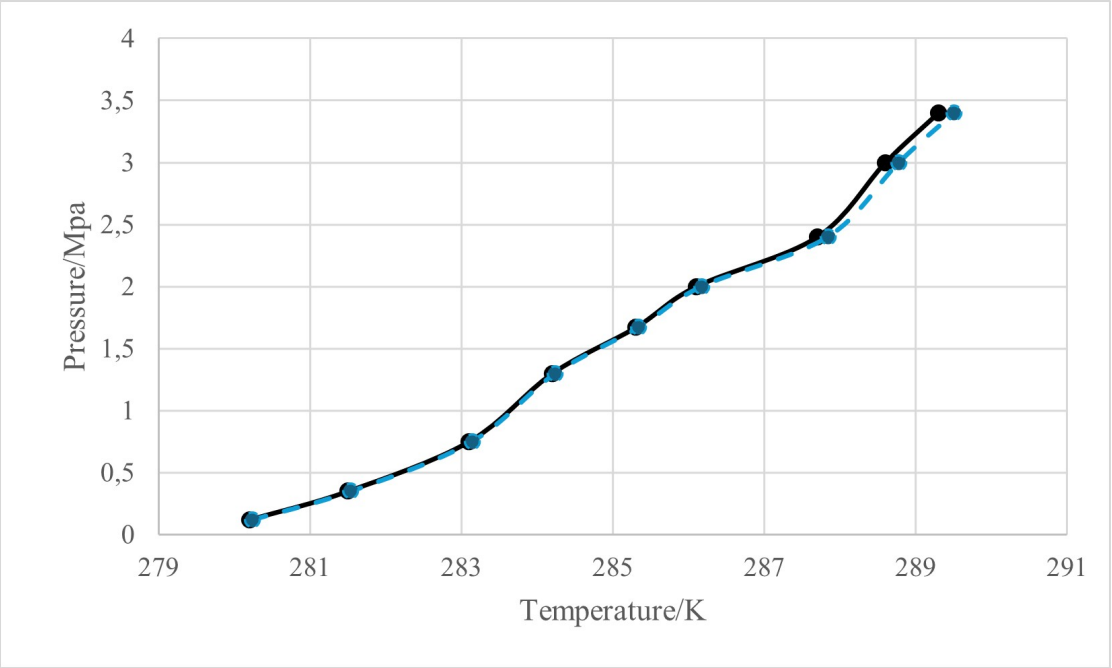

Figure 3.5: N_2 + Cp clathrate formation curve; black curve: experimental data, blue curve: Van der Waals and Platteuw model data.

Finally, it can be shown that the use of cyclopentane leads to very favorable conditions for clathrate formation. This line of research was later extended by introducing molar compositions of salts into the system.

The literature already reports several studies discussing hydrate formation in the presence of salts, carbon dioxide, and cyclopentane (as well as other promoters used in the past). However, the complex system that also includes nitrogen has not yet been fully investigated. One of the next logical steps is therefore to attempt the design of a more representative ternary system among the molecules considered in this paper, to integrate it within the Platteeuw and van der Waals model, and to introduce salt concentrations—through the use of appropriate mathematical coefficients—that could eventually reproduce real systems.

With regard to potential guest molecules, one can refer, for example, to the work of Le Quang et al. [47], where light hydrocarbons such as methane and ethane are added to the equilibrium conditions under study. Beyond hydrocarbons, equilibria can also be achieved with salts commonly encountered in everyday water treatment processes, such as NaCl and KCl, as investigated by Babakhani et al. [48]. These equilibria are explored mainly from an experimental standpoint, with the goal of enhancing the performance of this innovative technology. Nevertheless, efforts are also being made on the mathematical side to predict experimental behavior and

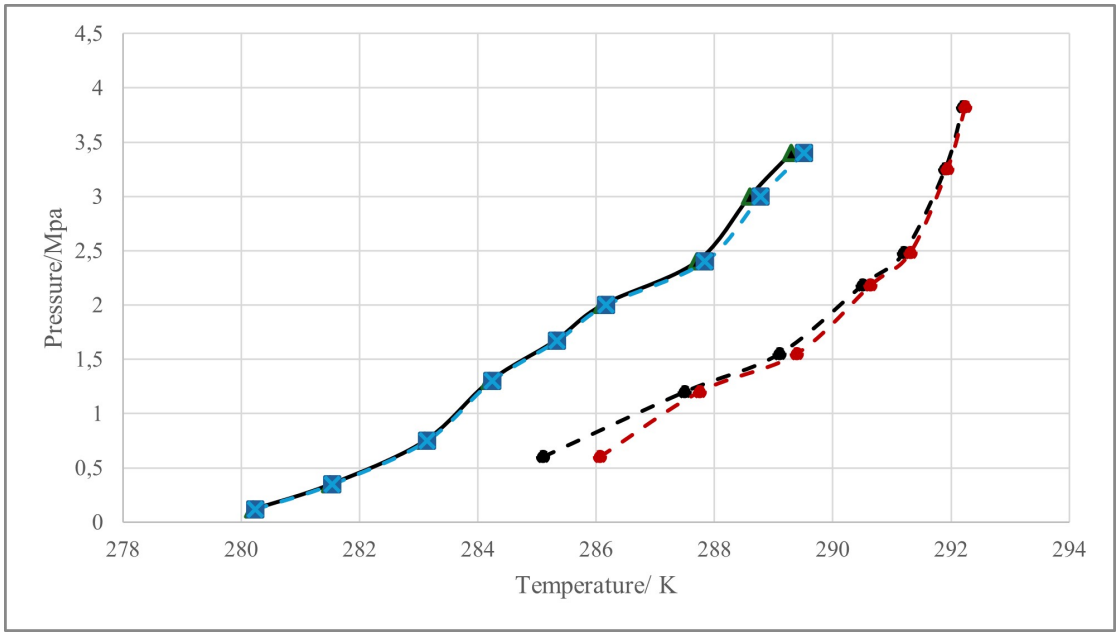

Figure 3.6: Comparison of hydrate formation curves: CO_2–Cp system (black dashed line) and N_2–Cp system (blue symbols with continuous black line).

identify the most suitable model. In this regard, the Platteeuw and van der Waals approach represents an excellent candidate for advancing these studies.

Chapter 4

Conclusion

These theoretical simulations, carried out using alternative and innovative models, have shown that the equilibria analyzed among cyclopentane, carbon dioxide, and nitrogen—initially under simple binary equilibrium conditions in liquid and gaseous phases as pure components, and later under conditions of clathrate hydrate formation—prove to be efficient and comparable with experimental data.

The results obtained with the PR78 model, thanks to the different calculation of binary coefficients that become dependent on operating conditions, are the most efficient, ensuring equilibrium even with molecules of very different characteristics. In fact, the model, mainly used for the calculation of fugacity coefficients, also provides excellent results in the calculation of equilibria during hydrate formation. The only system for which it was not possible to trace a curve as operating conditions varied was that of carbon dioxide and nitrogen, due to the lack of actual experimental data and its complexity.

Moreover, in order to attempt to create a ternary system among the three molecules, it would be necessary to further investigate the equilibrium of the system under consideration and, subsequently, during the calculation of hydrate formation, introduce different amounts of salts and compare them with experimental data.

Biblyography

[1] M. Pedro-Monzonís, A. Solera, J. Ferrer, T. Estrela e J. Paredes-Arquiola. «A review of water scarcity and drought indexes in water resources planning and management». In: *J. Hydrol.* (2015) (cit. a p. 1).

[2] A.D. Khawaji, I.K. Kutubkhanah e J.M. Wie. «Advances in seawater desalination technologies». In: *Desalination* (2008) (cit. a p. 1).

[3] K. Watkins. *Human Development Report - Beyond Scarcity: Power, Poverty and the Global Water Crisis*. Cambridge University Press, 2006 (cit. a p. 1).

[4] M.A. Montgomery e M. Elimelech. «Water and sanitation in developing countries: including health in the equation». In: *Environ. Sci. Technol.* (2007) (cit. a p. 1).

[5] U. Caldera, D. Bogdanov, S. Afanasyeva e C. Breyer. «Role of Seawater Desalination in the Management of an Integrated Water and 100% Renewable Energy Based Power Sector in Saudi Arabia». In: *Water* 10 (2017) (cit. a p. 1).

[6] M. Bert, O. Davidson, H. De Coninck, M. Meyer e L. Leo. *IPCC Special Report on Carbon Dioxide Capture and Storage*. New York: Cambridge University Press, 2005 (cit. a p. 1).

[7] Z.H. Zhou, J.H. Yang, Y. Zhang, L.F. Chang, W. Sun e J.Q. Wang. «NaA zeolite/carbon nanocomposite thin films with high permeance for CO2/N2 separation». In: (2007) (cit. a p. 1).

[8] S.M. Lu, Y.G. Ma, C.Y. Zhu e S.H. Shen. «The enhancement of CO2 chemical absorption by K2CO3 aqueous solution in the presence of activated carbon particles». In: *Chin. J. Chem. Eng.* (2007) (cit. a p. 1).

[9] Z. Li, J.H. Yao, Y. Wang e Y.P. Zhou. «Estimation of pore size distribution by CO2 adsorption and its application in physical activation of precursors». In: *Chin. J. Chem. Eng.* (2000) (cit. a p. 1).

[10] E. Sloan. *Clathrate Hydrates of Natural Gases*. 2nd. New York: Marcel Dekker, 1998 (cit. a p. 1).

[11] S. HoVan, B. Bouillot, J. Douzet, S. Maghsoodloo e J.M. Herr. «Experimental Measurement and Thermodynamic Modeling of Cyclopentane Hydrates with NaCl, KCl, CaCl2 or NaClKCl Present». In: (2017) (cit. alle pp. 2, 8).

[12] S. Kaur e B. P. Akhouri. «IOP Conference Series: Materials Science and Engineering». In: *IOP Conference Series: Materials Science and Engineering*. Vol. 1091. IOP Publishing, 2021, p. 012019 (cit. a p. 3).

[13] Chung-Tong Lin e Thomas E. Daubert. «Estimation of Partial Molar Volume and Fugacity Coefficient of Components in Mixtures from the Soave and Peng-Robinson Equations of State». In: (1978) (cit. a p. 4).

[14] J. M. Prausnitz, R. N. Lichtenthaler e E. G. Azevedo. *Molecular Thermodynamics of Fluid-Phase Equilibria*. 3rd. Prentice Hall, 1998 (cit. a p. 4).

[15] J. O. Valderrama. «A generalized cubic equation of state for thermodynamic property calculation». In: *Ind. Eng. Chem. Res.* 42 (2003), pp. 1603–1610 (cit. a p. 5).

[16] S. Vitu, J.-N. Jaubert, J. Pauly e J.-L. Daridon. «Thermodynamic study of mixtures with supercritical fluids: Part I». In: *J. Chem. Thermodyn.* (2008) (cit. a p. 5).

[17] S. Vitu, J.-N. Jaubert, J. Pauly, J.-L. Daridon e D. Barth. «Thermodynamic study of mixtures with supercritical fluids: Part II». In: *J. Supercrit. Fluids* (2008) (cit. a p. 5).

[18] S. Vitu, R. Privat e J.-N. Jaubert. «Phase equilibria modeling with cubic equations of state». In: *J. Supercrit. Fluids* (2008) (cit. a p. 5).

[19] D.-Y. Peng e D. B. Robinson. «A New Two-Constant Equation of State». In: *Industrial & Engineering Chemistry Fundamentals* 15.1 (1976), pp. 59–64 (cit. a p. 5).

[20] Jean-Noël Jaubert e Fabrice Mutelet. «VLE predictions with the Peng–Robinson equation of state and temperature dependent k_{ij} $calculatedthroughagroupcontributionmeth$ In: *Fluid Phase Equilibria* 224.2 (2004), pp. 285–304 (cit. alle pp. 6, 7).

[21] Romain Privat, Jean-Noël Jaubert e Fabrice Mutelet. «Addition of the Nitrogen Group to the PPR78 Model (Predictive 1978, Peng–Robinson EOS with Temperature-Dependent k_{ij} $CalculatedthroughaGroupContributionMethod$)» In: *Ind. Eng. Chem. Res.* 49.9 (2010), pp. 4606–4613 (cit. a p. 7).

[22] Andre F. Young, Fernando L. P. Pessoa e Victor R. R. Ahon. «Comparison of volume translation and covolume functions applied in the Peng–Robinson EoS for volumetric corrections». In: *Fluid Phase Equilibria* 425 (2016), pp. 390–399 (cit. a p. 7).

[23] Carl L. Yaws. *Critical Properties and Acentric Factor – Organic Compounds*. Knovel, 2009 (cit. a p. 7).

[24] Morteza Aminnaji, M. Fahed Qureshi, Hossein Dashti, Alfred Hase, Abdolali Mosalanejad, Amir Jahanbakhsh, Masoud Babaei, Amirpiran Amiri e Mercedes Maroto-Valer. «CO2 Gas Hydrate for Carbon Capture and Storage Applications – Part 1». In: *Energy* (2024). In press, Journal Pre-proof. DOI: 10.1016/j.energy.2024.131579. URL: https://doi.org/10.1016/j.energy.2024.131579 (cit. a p. 8).

[25] A. T. Trueba, L. J. Rovetto, L. J. Florusse, M. C. Kroon e C. J. Peters. «Phase equilibrium measurements of structure II clathrate hydrates of hydrogen with various promoters». In: *Fluid Phase Equilibria* 307 (2011), pp. 6–10. DOI: 10.1016/j.fluid.2011.04.025. URL: https://doi.org/10.1016/j.fluid.2011.04.025 (cit. a p. 8).

[26] Aleksander Kreglewski e Kenneth R. Hall. «Phase Equilibria Calculated for the Systems N_2 + CO_2, CH_4 + CO_2 and CH_4 + H_2S». In: *Fluid Phase Equilibria* 15 (1983). Thermodynamics Research Center, Texas AM University, College Station, TX 77843, U.S.A., pp. 1–32 (cit. alle pp. 9, 11, 13, 15, 16).

[27] Jürgen Stoll, Jadran Vrabec e Hans Hasse. «Vapor–liquid equilibria of mixtures containing nitrogen, oxygen, carbon dioxide, and ethane». In: *AIChE Journal* (2004). First published: 16 April 2004. DOI: 10.1002/aic.690490826 (cit. alle pp. 9, 10).

[28] Nilesh N. Shah, John A. Zollweg e William B. Streett. «Vapor-liquid equilibrium in the system carbon dioxide + cyclopentane from 275 to 493 K at pressures to 12.2 MPa». In: *Journal of Chemical Engineering Data* 36.2 (apr. 1991) (cit. alle pp. 15, 17, 18).

[29] Sergiu Sima, Julia Cruz-Doblas, Martin Cismondi e Catinca Secuianu. «High-pressure phase equilibrium calculations for carbon dioxide + cyclopentane binary system». In: *Central European Journal of Chemistry* 12 (gen. 2014), pp. 918–927 (cit. alle pp. 15, 17, 18).

[30] Pradeep Marathe e Stanley I. Sandler. «High-pressure vapor-liquid equilibrium of some binary mixtures of cyclopentane, argon, nitrogen, N-butane, and neopentane». In: *Journal of Chemical Engineering Data* 36.2 (apr. 1991) (cit. a p. 19).

[31] Romain Privat, Jean-Noël Jaubert e Fabrice Mutelet. «Addition of the Nitrogen Group to the PPR78 Model (Predictive 1978, Peng Robinson EOS with Temperature-Dependent k_{ij} Calculated through a Group Contribution Method)». In: *Journal of Chemical & Engineering Data* 54.3 (2009), pp. 1153–1165. DOI: 10.1021/je8006329 (cit. a p. 20).

[32] J.-M. Herri, A. Bouchemoua, M. Kwaterski, A. Fezoua, Y. Ouabbas e A. Cameirao. «Gas hydrate equilibria for CO2–N2 and CO2–CH4 gas mixtures — Experimental studies and thermodynamic modelling». In: *Fluid Phase Equilibria* 301.2 (2011), pp. 171–190. DOI: 10.1016/j.fluid.2010.12.024 (cit. a p. 24).

[33] W.R. Parrish e J.M. Prausnitz. «Dissociation Pressures of Gas Hydrates Formed by Gas Mixtures». In: *Industrial & Engineering Chemistry Process Design and Development* 11.1 (1972), pp. 26–35. DOI: 10.1021/i260041a006 (cit. a p. 25).

[34] P.J. Herslund, K. Thomsen, J. Abildskov et al. «Thermodynamic Promotion of Carbon Dioxide-Clathrate Hydrate Formation by Tetrahydrofuran, Cyclopentane and Their Mixtures». In: *Energy & Fuels* 17 (2013), pp. XXXX–XXXX (cit. a p. 25).

[35] J.-M. Herri e E. Chassefière. «Carbon dioxide, argon, nitrogen and methane clathrate hydrates: Thermodynamic modelling, investigation of their stability in Martian atmospheric conditions and variability of methane trapping». In: *Planetary and Space Science* 73.1 (2012), pp. 376–386. DOI: 10.1016/j.pss.2012.08.013 (cit. a p. 25).

[36] S. Muromachi, H.D. Nagashima, J.-M. Herri e R. Ohmura. «Thermodynamic modeling for clathrate hydrates of ozone». In: *Journal of Chemical Thermodynamics* 64 (2013), pp. 193–197. DOI: 10.1016/j.jct.2013.04.008 (cit. a p. 25).

[37] D. Le Quang, B. Bouillot, J.-M. Herri, P. Glenat e P. Duchet-Suchaux. «Experimental procedure and results to measure the composition of gas hydrate, during crystallization and at equilibrium, from N2–CO2–CH4–C2H6–C3H8–C4H10 gas mixtures». In: *Fluid Phase Equilibria* 413 (2016), pp. 10–21. DOI: 10.1016/j.fluid.2015.09.029 (cit. a p. 25).

[38] Y.P. Handa e J.S. Tse. «Thermodynamic Properties of Empty Lattices of Structure I and Structure II Clathrate Hydrate». In: *The Journal of Physical Chemistry* 90.22 (1986), pp. 5917–5921. DOI: 10.1021/j100414a014 (cit. alle pp. 25, 26).

[39] J.-M. Herri, A. Bouchemoua, M. Kwaterski, A. Fezoua, Y. Ouabbas e A. Cameirao. «Gas hydrate equilibria for CO2–N2 and CO2–CH4 gas mixtures — Experimental studies and thermodynamic modelling». In: *Fluid Phase Equilibria* 301.2 (2011), pp. 171–190. DOI: 10.1016/j.fluid.2010.12.024 (cit. alle pp. 25, 27).

[40] L.S. Tee, S. Gotoh e W.E. Stewart. «Molecular Parameters for Normal Fluids. Kihara Potential with Spherical Core». In: *Industrial & Engineering Chemistry Fundamentals* 5.3 (1966), pp. 363–367. DOI: 10.1021/i160018a011 (cit. a p. 26).

[41] E.D. Sloan. *Clathrate Hydrates of Natural Gases*. 2nd. Vol. 14. Chemical Industries Series. New York: Marcel Dekker, 2000 (cit. a p. 26).

[42] E.D. Sloan e C.A. Koh. *Clathrate Hydrates of Natural Gases*. 3rd. Boca Raton, FL: Taylor & Francis Group, 2008 (cit. a p. 26).

[43] E.D. Sloan. *Clathrate Hydrates of Natural Gases*. 2nd. New York: Marcel Dekker, 1998 (cit. a p. 26).

[44] S. Maghsoodloo Babakhani, S. Ho-van, B. Bouillot, J. Douzet e J.-M. Herri. «Phase equilibrium measurements and modelling of mixed cyclopentane and carbon dioxide hydrates in presence of salts». In: *Chemical Engineering Science* 214 (2020) (cit. a p. 27).

[45] Jean-Michel Herri, Amina Bouchemoua-Benaissa, Matthias Kwaterski, Amara Fezoua, Yamina Ouabbas e Ana Cameirão. «Gas hydrate equilibria for CO_2–N_2 and CO_2–CH_4 gas mixtures—Experimental studies and thermodynamic modelling». In: *Fluid Phase Equilibria* 301 (2011), pp. 171–190. DOI: 10.1016/j.fluid.2010.12.001 (cit. a p. 27).

[46] J. Zhang e J. W. Lee. «Equilibrium of hydrogen + cyclopentane and carbon dioxide + cyclopentane binary hydrates». In: *Journal of Chemical & Engineering Data* 54.2 (2008), pp. 659–661. DOI: 10.1021/je7005644 (cit. a p. 31).

[47] Baptiste Bouillot, Duyen Le Quang, Quang-Du Le, Jean-Michel Herri, Philippe Glenat e Pierre Duchet-Suchaux. «Experimental procedure and results to measure the composition of gas hydrate, during crystallization and at equilibrium, from N2–CO2–CH4–C2H6–C3H8–C4H10 gas mixtures». In: *Proceedings of the 8th International Conference on Gas Hydrates (ICGH8)*. HAL preprint: hal-01066933. Beijing, China, lug. 2014, T1–71 (cit. a p. 33).

[48] Saheb Maghsoodloo Babakhani, Son Ho-Van, Baptiste Bouillot, Jérôme Douzet e Jean-Michel Herri. «Phase equilibrium measurements and modelling of mixed cyclopentane and carbon dioxide hydrates in presence of salts». In: *Chemical Engineering Science* (2019). Journal Pre-Proofs. DOI: 10.1016/j.ces.2019.115442 (cit. a p. 33).

Ringraziamenti